

NASA TECHNICAL MEMORANDUM

NASA TM X-64857

A STANDARD PARTICLE SIZER-VELOCIMETER

By Adarsh Deepak, R. Ozarski, and J. A. L. Thomson
Systems Dynamics Laboratory

June 1974

(NASA-TM-X-64857) A STANDARD PARTICLE
SIZER-VELOCIMETER (NASA)

N74-28937

G3/14 Unclass
43493

NASA

*George C. Marshall Space Flight Center
Marshall Space Flight Center, Alabama*

Reproduced by
NATIONAL TECHNICAL
INFORMATION SERVICE
US Department of Commerce
Springfield, VA. 22151

1. Report No. NASA TM X - 64857		2. Government Accession No.	3. Recipient's Catalog No.
4. Title and Subtitle A Standard Particle Sizer - Velocimeter		5. Report Date June 1974	
		6. Performing Organization Code	
7. Author(s) A. Deepak*, R. Ozarski**, and J. A. L. Thomson***		8. Performing Organization Report No.	
9. Performing Organization Name and Address George C. Marshall Space Flight Center Marshall Space Flight Center, Alabama 35812		10. Work Unit No.	
		11. Contract or Grant No. NAS 8-24810 (Tech. Monitor, R. M. Huffaker)	
12. Sponsoring Agency Name and Address National Aeronautics and Space Administration Washington, D. C. 20546		13. Type of Report and Period Covered Technical Memorandum	
		14. Sponsoring Agency Code	
15. Supplementary Notes Prepared by Systems Dynamics Laboratory, Science and Engineering *National Academy of Sciences Postdoctoral Resident Research Associate **Research Institute for Engineering Sciences (RIES), Wayne State University, Detroit, MI ***Physical Dynamics, Inc., Berkeley, CA			
16. Abstract This report describes a standard particle sizer-cum-velocimeter designed and build for the purpose of providing a standard source of aerosols of known size-distribution, moving with a known velocity, for the purpose of calibrating the continuous wave (CW) CO ₂ - Laser Doppler Velocimeters at Marshall Space Flight Center. The instrument is designed with the capabilities of: (1) monitoring the size-distribution of particles of diameters larger than 1.0 μ m; (2) measuring flow velocities in the range 0.05 - 100.0 cm/sec; (3) photographing particles of diameters above 0.2 μ m moving at slow speeds (\sim 0.1 cm/sec); (4) measuring the size-distribution of particles settling in quiet air (or convection velocities of less than 0.15 cm/sec); (5) use in the laboratory or in the field. The instrument is made up of the laser scattering counter (LSC) and the photographic system, each of which can function independently or in conjunction for simultaneous monitoring of the same sample of particles. The LSC can be easily modified to operate in two modes: (1) as a forward-scattering particle sizer-counter or (2) as a forward dual-beam velocimeter. The two modes of operation of the LSC are described in detail, though the experimental results of its use as a velocimeter are not reported here. <div style="text-align: center;">PRICES SUBJECT TO CHANGE</div>			
17. Key Words (Suggested by Author(s))		18. Distribution Statement Unclassified-unlimited J. A. Lovingood Director, Systems Dynamics Laboratory	
19. Security Classif. (of this report) Unclassified		20. Security Classif. (of this page) Unclassified	

TABLE OF CONTENTS

	Page
INTRODUCTION	1
BRIEF DESCRIPTION OF THE INSTRUMENT	2
The Photographic System	2
The Laser Scattering Counter	4
THE PARTICLE SIZING COUNTER	6
A Simple Theoretical Evaluation of the S/N for a Single Scatterer For the Two Modes of Operation	6
Analysis of the Inversion Problem: Inverting the Signal Data to Particle Size-Distributions, $n(r)$	10
The Inversion Problem.	16
Experimental Results	24
THE DUAL-BEAM VELOCIMETER	24
The Theoretical Analysis.	24
CONCLUSIONS	30
REFERENCES	52

PRECEDING PAGE BLANK NOT FILMED

LIST OF ILLUSTRATIONS

Figure	Title	Page
1a.	Plan of the sizer-velocimeter	32
1b.	Side view of the laser scattering counter (LSC)	32
2a.	The photographic system and the LSC fitted together for simultaneous operation	33
2b.	Details of the photographic system when used in conjunction with the LSC	33
2c.	Glass chamber fitted for simultaneous operation of the photographic system and the LSC	34
3.	Plan of the instrumentation	35
4.	Schematic diagram of the LSC optics	35
5.	Optical schematic of the LSC and photographic system used in conjunction	36
6.	Stokes' velocity versus radius	37
7.	Schematic illustration of the method	38
8.	Schematic diagram of the photographic system	39
9.	Acetone and dry ice pump	39
10.	Graph of $n(r)$ versus r for Al_2O_3 particles of (supplier quoted) radius of 1.5 microns	40
11.	LSC used as a fringe-system counter	41
12.	Polar diagram of the light scattered by a Mie-particle	41
13.	Schematic diagram of the LSC collecting lens	41

LIST OF ILLUSTRATIONS (Concluded)

Figure	Title	Page
14a.	Schematic of the intensity distribution at the focal volume for a spherical focusing lens	42
14b.	Schematic of the intensity distribution at the focal volume for a cylindrical focusing lens	43
15.	Contours of constant intensity as a function of x and r	44
16a.	Graph of $N_s(I)$ versus I for the Al_2O_3 particles of 1.5 microns radius	45
16b.	Graphs of N_s versus I and n_s versus i ($i = \sqrt{I}$) for aerosols in closed room ambient air	46
17a.	Focal volume dimensions	47
17b.	Two-beam diffraction pattern at the focus	47
17c.	The beam crossover region, where $\theta = \frac{D}{f}$	47
18.	Schematic of intensity patterns for the trajectories of two particles: particle 1 through the focal volume; particle 2 through the non-focal region	48
19.	Schematic of intensity patterns for two particles passing through various regions of the dual beam system	49
20.	Shape of one-fourth of the crossover region in three dimensions for the cylindrical focusing lens	50
21.	The power spectrum	50

LIST OF TABLES

Table	Title	Page
1.	Values of S/N for Various Size Particles	51

BRIEF DESCRIPTION OF THE INSTRUMENT

The instrument is made up of two parts: (1) the laser scattering counter (LSC), and (2), the photographic system, both of which can function as independent units or can be fitted together to monitor simultaneously the same sample of particles. In the latter case, the particles pass through the common overlapping portion of the sensing (focal) volumes of the two units. (Figs. 1 through 5). Their test section is a 15.24-cm-diameter aperture into which a glass cell (or a wind-tunnel section) can be installed.

The instrument is sturdily built yet light enough for field use and ease of portability. Both parts are mounted between two parallel aluminum sheets (3.1-mm-thick) held 12.5 cm apart by aluminum rods to form sturdy units for field use. The two units can be fitted together for simultaneous use on a sample of particles. The specifications for the various components of the two parts were obtained by theoretical analysis of the techniques involved. Simple analyses of the LSC used as a sizer-counter or as a velocimeter are described in later sections. The analysis of the photographic technique is described in detail in an earlier paper [1].

The Photographic System

The details of this system are described in Reference 1. However, a brief description of the photographic system is given below. This technique provides an (absolute) method for measuring aerosol size-distributions that is independent of the light-scattering properties of the particles.

The basis of the method is the Stokes' law [2], which relates the terminal velocity (v_s) of a sphere settling freely in a quiet medium to its radius r and is given by the expression

$$v_s = \frac{2}{9 \eta_m} (\rho_p - \rho_m) g r^2 \quad (1)$$

where ρ_p and ρ_m represent the specific gravity of the sphere and the medium, respectively, g is the acceleration due to gravity and η_m is the viscosity of the medium. v_s is also referred to as the Stokes' velocity. The values of

STANDARD PARTICLE SIZER-VELOCIMETER (SPSV)

INTRODUCTION

The primary aim of the research, design, and construction of a standard particle sizer-velocimeter (SPSV) was to provide a standard source of aerosols of known size-distribution moving with a known velocity for the purpose of calibrating the continuous wave (CW) CO₂-Laser Doppler Velocimeters built at Marshall Space Flight Center. However, the instrument can also be adapted for (1) use in determining the size-distribution and velocity of particulates in water or other fluids; (2) the photographic study of vortex formations, etc.; and (3) the study of acoustic coagulation of aerosols, etc.

The following main objectives were to be incorporated in the construction of this instrument:

- (1) It should be capable of monitoring the size of particles having diameters larger than 1.0 μm , provided the particles can be assumed to be spherical.
- (2) It should be capable of measuring the flow velocities from 0.05 cm/sec to 100 cm/sec.
- (3) It should be possible to photograph particles with diameters above 0.2 μm , provided they are very slow moving, typically 0.1 cm/sec.
- (4) It should be a portable instrument, capable of being used in the field under real atmospheric conditions.
- (5) The test section of the instrument through which particles move should be of sufficient size (up to 15.24-cm-diameter) that it can accommodate at its center the focal volume of the CW CO₂-Laser Doppler Velocimeter at a distance of 100 feet.

An instrument was designed and built with the above objectives in mind and successfully tested for its performance. The results were quite gratifying considering that this was a first generation study and that the instrument was built with economy-priced equipment that was easily accessible. The theory and the description of the instrument are contained in the following sections.

v_s versus r , for the aluminum (Al_2O_3) particles ($\rho_p = 3.965$) settling in air ($\rho_m = 1.22 \times 10^{-3}$, $\eta_m = 1.898 \times 10^{-4}$ poise), and water ($\eta_m = 0.01$ poise, $\rho_m = 1.0$), and for fog particles settling in air are represented graphically in Figure 6.

Aerosol particles are allowed to fall freely in a vertical glass walled cell (Fig. 7) in which the convection currents have been reduced to a minimum. The settling velocity of the particles is determined by photographing them while the light entering the lens is chopped at a known rate. The particles are illuminated by a 1-mm vertical sheet or slab of light projected into the cell. A camera aimed perpendicular to the slab of light photographs the particle tracks (typical exposure times are 0.5 or 1.0 sec). The image of the falling particle is thus a series of dashes. The velocity of fall can then be measured from the spacing of the dashes.

The velocity thus measured is the sum of the Stokes' velocity and the convection velocity. It is the experimental suppression of the convection currents and the theoretical elimination of their efforts that is the major cause of the complexity of the experiment and of the limiting of method to large particles. The procedures for damping the convection currents are described in Reference 1.

DOP particles ($0.3 \mu\text{m}$) move essentially with the convection air currents and so can be used to measure the vertical component of convection velocities, which can then be subtracted from the vertical component of the total velocity of large particles to obtain their true Stokes' velocity.

When functioning as an independent unit, the instrumental set-up essentially consists of a vertical glass-walled cell and a photographic system (Fig. 8).

The cell is a vertical glass-walled chamber which has airtight joints and can be closed off airtight at the top and bottom. Its crosssection is octagonal. Each side is 5 cm wide by 45 cm high. Its walls are covered on the inside with flock paper, except for the appropriate 5-cm-diameter openings for the passage of projected light and for the camera lens. This helps to minimize the extraneous light entering the lens, and provides a dark backdrop to the illuminated particles. The bottom is closed off by inserting a 2.5-cm-thick aluminum plate which is cooled to and maintained at the steady temperature of dry ice (-12°C) over its entire surface by circulating a CO_2 and Acetone mixture from a dry ice and Acetone pump (Fig. 9).

The photographic system consists of a source of light, a camera with a bellows, and a uniformly rotating chopper. The source of light is a 500-W slide projector (Bell and Howell), with a rectangular aperture ($1\text{ mm} \times 3.81\text{ cm}$) inserted in the position of a slide. The beam of light is projected through a short-focused convex lens (f/z) to form a sharp focus of the aperture at the center of the cell. Near the focus a vertical sheet or slab of light 1 mm thick illuminates the falling particles. The depth of focus is about 5 mm . The camera unit is a $f/1.7$ Minolta lens mounted in front of a bellows, and the entire unit is fixed to the external framework. The bellows is adjusted to obtain a sharp image of an illuminated object at the position of the projector beam focus, about 8.75 cm in front of the lens, so that magnification of nearly unity can be obtained. Typically, the magnification is about 0.8 . The camera body can be attached to or removed from the bellows unit for film loading or unloading.

A uniformly rotating chopper is used just in front of the lens, in order to accurately select and measure the particle track lengths in the photographs. With the help of a belt-and-pully arrangement the chopper (2 or 4 blades) is rotated by a small synchronous electric motor (300 rpm) fixed to the external framework. By choosing an appropriate combination of pulleys and chopper blades, different chopping rates can be obtained. Typical values are 10 or 100 chops/sec.

Tri-X (ASA 400) film was found to be the most suitable film as far as its speed, resolving power and ease of developing are concerned. It is sensitive (fast) enough to record tracks of particles with diameters as low as $0.3\text{ }\mu\text{m}$, often moving with velocities as high as 3 mm/sec , when the bellows is set for a magnification of about 0.8 .

Several experiments were performed with Al_2O_3 particles (of diameters $0.3\text{ }\mu\text{m}$, $1.0\text{ }\mu\text{m}$, $3.0\text{ }\mu\text{m}$, and $8.0\text{ }\mu\text{m}$). Results of a typical experiment with a sample of $3.0\text{-}\mu\text{m}$ -diameter Al_2O_3 particles (value supplied by the manufacturer), are shown in Figure 10. For details see Reference 1.

The Laser Scattering Counter

The laser scattering counter (LSC) consists essentially of a 1-mW power He-Ne laser, input optics, collecting optics, photo-detector and signal-processing electronics. It is a forward scattering type of an instrument in which the forward scattered light is collected by a high quality camera lens while the direct beam is stopped.

By changing the configuration of the input optics and signal processing electronics, the instrument can be used in two modes of operation, namely as (1) a forward-scattering particle-sizing counter; and, (2) a dual-beam velocimeter.

The only difference in the two modes lies in the pre-focus optics and the signal processing electronics. In the former case, the laser beam (1-mm diameter) is focused by a cylindrical lens ($f = 9.4 \text{ cm}$ to an astigmatic focal volume $(0.06 \text{ mm} \times 1 \text{ mm}$ in cross section). In the latter case, a beam-splitter unit (Fig. 11) consisting of a partially silvered glass plate and a plane mirror, is inserted in the path of the beam, making sure that in doing so the position of the focal point remains the same, so that no other part of the whole optical system needs realignment. Also, in the former case, the photo-detector (RCA 931A photomultiplier) is used as a signal strength detector. The pulses of scattered light produced by the passage of particles are converted by the PM tube to electrical signals which are then either recorded on a chart recorder (as in our case) or analyzed and counted by electronic circuits; signal (amplitude) height yields the particle size. In the latter, the circuitry and processing electronics are changed to use the PM as a frequency mixer; the modulation frequency or the "beat" frequency yields the particle velocity. A frequency spectrum analyzer is used for this purpose.

The collecting optics consist of a good quality camera lens (Honeywell Pentax, $f = 50 \text{ mm}$, $f/1.4$), a direct-beam stop, a glass micro-slide and an exit pupil (Fig. 1 through 3). The direct beam is stopped by a blackened spot (0.63 cm diameter) on a thin acetate disc attached in front of the lens, so that only the light scattered in the forward cone is collected by the lens. The efficient trapping of the unused illumination is important, as the ultimate sensitivity of the instrument is determined by the power S/N, and this is determined largely by the trap efficiency. The collected scattered light is focused in the center of a very small aperture ($0.5 \text{ mm} \times 0.5 \text{ mm}$) A_1 , placed a little distance in front of the PM. By selecting the correct combination of the f-no. of the camera lens and the size of the exit aperture, the desired effective measuring volume of the test particles can be selected (typical value of the depth of focus of lens is about 2mm in this case). A thin micro-slide placed in between the lens and the exit pupil (Figs. 2,3,4) can be rotated on its vertical axis to make the fine translational adjustment of the focused image in the plane of the exit pupil.

A theoretical analysis for the two modes of operation is given in the following sections.

THE PARTICLE SIZING COUNTER

A Simple Theoretical Evaluation of the S/N for a Single Scatterer For the Two Modes of Operation

If the laser (wavelength λ) beam diameter is D_B , and the focal length of the cylindrical lens is f_{CL} , then, at the waist of the focal volume the width is

$$\delta = (\lambda f_{CL} / D_B) , \quad (2)$$

which yields an area of cross-section of

$$A_L = \delta \times D_B . \quad (3)$$

Let the laser power be P_L , then irradiance at the focal waist is

$$I_0 = P_L / A_L . \quad (4)$$

Let a particle of diameter d (cm) traverse the focal width δ (cm) with a velocity v (cm/sec). Then, the particle remains inside the beam for a time

$$t = (\delta / v) , \text{sec} \quad (5)$$

and the total number of photons scattered by the particle in all directions is

$$\begin{aligned} N_{SC} &= \sigma_T \times I_0 \text{ (watts/cm}^2\text{)} \times (\lambda \text{ (cm)} / 2 \times 10^{-19} \text{ joules)} \times t \\ &= \frac{\pi d^2}{4} Q(x) \times (P_L / A_L) \times (\lambda / 2 \times 10^{-19}) \times \delta / v , \end{aligned} \quad (6)$$

where $Q(x)$, the efficiency factor, $= \sigma_T / \pi r^2$, σ_T is the total scattering cross-section; and the number of photons scattered per unit solid angle is

$$\frac{dN_{SC}}{d\Omega} = \left(\frac{d\sigma}{d\Omega} \right) \times I_0 \times (\lambda/2 \times 10^{-19}) \times (\delta/v) \quad . \quad (7)$$

We can approximately calculate $\left(\frac{d\sigma}{d\Omega} \right)$ for the forward scattered light from the fact that about 84 percent of the total scattered light is contained in the forward scattering lobe (Fig. 12). Thus,

$$\frac{d\sigma}{d\Omega} = 0.84 (\sigma_T / \Omega_F) \quad , \quad (8)$$

where Ω_F is the solid angle for the forward lobe. The forward lobe of scattered light is contained within an angle $2\theta_F$, where the forward scattering angle θ_F is given by the relation

$$\theta_F = [35/d (\mu m)] \text{ degrees} \quad , \quad (9)$$

for which the solid angle is

$$\Omega_F = \pi \left(\frac{\theta_F \text{ degrees}}{57.3} \right)^2 \simeq \pi (0.4/d_\mu^2) \quad . \quad (10)$$

Thus,

$$\begin{aligned} \left(\frac{d\sigma}{d\Omega} \right)_F &= 0.84 \times (\pi d^2 \times 10^{-8} Q(x) / 4.0) \times (d_\mu^2 / 0.4) \\ &= 1.6 \times 10^{-18} Q(x) d_\mu^4 (\text{cm}^2/\text{sr}) \quad . \end{aligned} \quad (11)$$

Hence, the number of photons scattered per unit solid angle in the forward direction is

$$\begin{aligned} \left(\frac{dN_{SC}}{d\Omega} \right)_F &\simeq \frac{P_L}{A_L} \times \frac{\lambda \text{ (cm)}}{2 \times 10^{-19}} \times \frac{\delta}{v} \times \left(\frac{d\sigma}{d\Omega} \right)_F \\ &\simeq 8 \times 10^{14} \cdot \frac{P_L \lambda}{v D_B} Q(x) d_\mu^4, \text{ (photons/sr).} \end{aligned} \quad (12)$$

COLLECTION OF SCATTERED PHOTONS (SIGNAL)

From Figure 13, the collecting solid angle,

$$\begin{aligned} \Omega_c &= \Omega_1 - \Omega_2 \\ &= \pi (\theta_1^2 - \theta_2^2) \\ &= \frac{\pi}{4 d_c^2} (D_c^2 - D_2^2). \end{aligned} \quad (13)$$

For

$$D_1 = 0.6 \text{ cm}, D_c = 3 \text{ cm}, \Omega_c = (6.5/d_c^2), \text{ sr}. \quad (14)$$

The number of scattered photons collected by the lens

$$\begin{aligned} N_{ph} &= \left(\frac{dN_{SC}}{d\Omega} \right)_F \Omega_c \\ &\simeq 8 \times 10^{14} \left[\frac{P_L \lambda}{v D_B} Q(x) d_\mu^2 \right] \left[\frac{6.5}{d_c^2} \right]. \end{aligned} \quad (15)$$

For

$$d_c = 10 \text{ cm} , \lambda = 0.63 \times 10^{-4} \text{ cm} , P_L = 10^{-3} \text{ W} ,$$

$$D_B = 0.1 \text{ cm}, f_{CL} = 3.75 \text{ in.} = 9.5 \text{ cm} ,$$

$$\left[\delta = \frac{\lambda f_{CL}}{D_B} = 60 \mu, A_L = 6 \times 10^{-4} \text{ cm}^2 \right] .$$

$$N_{ph} = 5.04 \times 10^8 \frac{Q(x) d^4}{v} , \text{ (photons)} . \quad (16)$$

For example, for

$$d_\mu = 3.0 \mu , x \sim 15.0 , Q(x) \sim 2 , (x = \pi d/\lambda)$$

$$v = 10^3 \text{ cm/s} , \text{ we obtain}$$

$$N_{ph} = 5 \times 10^6 \text{ photons}$$

Table 1 gives the values of N_{ph} for various values of d_μ and v .

Let the quantum-mechanical efficiency of the PM = η_{QM} . Then the number of photo-electrons produced,

$$N_e = \eta_{QM} \cdot N_{ph} . \quad (17)$$

Then, the

$$S/N \approx \sqrt{N_e} . \quad (18)$$

If

$$\eta_{QM} = 1\% , \quad N_e = 5 \times 10^6 \times 10^{-2} = 5 \times 10^4 ; \quad (19)$$

then

$$S/N = 5 \times 10^2 = 225 \quad (20)$$

Table 1 gives the S/N values for various size particles and different velocities.

Thus it is possible to detect a $3.0\mu\text{m}$ particles moving through the focal volume at a velocity of 10^3 cm/sec, with a relatively inexpensive PM tube such as the RCA 931 A used in the instrument.

Analysis of the Inversion Problem: Inverting the Signal Data to Particle Size-Distributions, $n(r)$

INTENSITY DISTRIBUTION

Before such an inversion can be performed, the spatial variation of the laser beam intensity (I) at the focal volume must be understood. The focal volumes of spherical lens and, a cylindrical lens are considered. For the sake of simplification, only the one-dimensional case of the variation along the beam direction is studied.

If the laser beam incident on the lens has a Gaussian intensity profile, then at the focal volume of both types of lenses, the intensity profile is Gaussian along the y-axis. However, in the x-direction the intensity curve is considered

to be Gaussian for a spherical lens, and a dispersion curve for a cylindrical lens.

We define the following set of three-parameter functions of radius r , distance x from the lens, and time t .

Size-Spatial Distribution. The size-spatial distribution, $\eta(r, x, t)$ is the number of particles per cubic centimeter per unit radius at radius r and per unit distance at x at time t . The units are $[\text{cm}^{-5}]$.

Cumulative Under-Size-Spatial Distribution. The cumulative under-size-spatial distribution, $N(r, x, t)$, is the number of particles per cubic centimeter having their radii less than r , their distance within x and their duration less than t ,

$$N(r, x, t) = \int_0^t \int_0^x \int_0^r \eta(r', x', t') dr' dx' dt', [\text{cm}^{-3}] \quad (21)$$

Thus, the number of particles per cubic centimeter having radii in the range of $(r', r' + dr')$, distance within $(x', x' + dx')$, and time within $(t', t' + dt')$ is

$$dN(r', x', t') = \eta(r', x', t') dr' dx' dt', [\text{cm}^{-3}] \quad (22)$$

Then the rate of flow of particles having radii within $(r', r' + dr')$ passing within $(x', x' + dx')$ is

$$\frac{dN(r', x', t')}{dt'} = \eta(r', x', t') dr' dx', [\text{cm}^{-3} \text{ sec}^{-1}] \quad (23)$$

For a steady flow, it is assumed that the size-distribution, $n(r)$, of the particles is independent of x and t , the function $\eta(r, x, t)$ becomes separable:

$$\eta(r, x, t) = n(r) N_o(x, t), [\text{cm}^{-5}] \quad (24)$$

where $N_o(x, t)$ is the total number of all particle of all sizes passing per unit length at distance x at time t . It has dimensions $[cm^{-1}]$. Since $n(r)$ is independent of x and t ,

$$\frac{d N_o(r', x', t')}{dt} = \dot{N}(r', x', t') = \dot{N}_o(x', t') n(r') dr' dx' [cm^{-3} sec^{-1}], \quad (25)$$

where

$$\dot{N}_o(x', t') = \frac{d N_o(x')}{dt}, [cm^{-1} sec^{-1}] \quad (26)$$

is rate of flow of particles of all sizes through a unit length at x' .

CASE 1: GAUSSIAN SPATIAL INTENSITY AT FOCAL VOLUME

Let the spatial-intensity distribution at the focus (Fig. 14) be given by

$$I_o e^{-\frac{(x-x_o)^2}{\delta^2}} \quad (27)$$

where δ is the focal width ($\delta = \lambda f/d$). Then the scattered signal flux (intensity) particle of radius r situated at position x is

$$I(r, x) = \sigma(r) I_o e^{-\frac{(x-x_o)^2}{\delta^2}}, [watts/(\Delta\lambda)] \quad (28)$$

where $\sigma(r)$ is the total scattering cross-section (cm^2) for a particle of radius r , and $x = x_0$ at the center of focal volume.

This relation can be graphically represented by a series of curves of constant scattered intensity, $I(r, x)$, by varying r and x . (Fig. 15).

For a particle of given radius r , in order to obtain a scattered intensity I , it must be at distance x from the lens, where

$$x = x_0 + \delta \sqrt{\frac{\ln I_0 \sigma(r)}{I}} . \quad (29)$$

To find the number per cubic centimeter of particles of all sizes anywhere within the depth of focus of the collecting lens which would give signals within the intensity ranges $(I, I + dI)$ in one second, let $\dot{n}_s(I)$ be the number of pulses of signal amplitude (I) recorded per second per unit signal amplitude. Then the number of pulses per second having amplitude in the range $(I, I + dI)$ is

$$\dot{n}_s(I) dI = \int_{r'} n(r') dr' \dot{N}_0'(t') \frac{dx'}{dI} dI , \quad (30)$$

where, it is assumed, $\dot{N}_0'(t')$ is a constant value for all positions x . Thus,

$$\dot{n}_s(I) = N_0'(t') \int_{r'} n(r') dr' \left(\frac{dx'}{dI} \right) . \quad (31)$$

From equation (29) we obtain

$$\frac{dx'}{dI} = \frac{\delta}{2I \sqrt{\ln \left[\frac{I_0 \sigma(r)}{I} \right]}} \quad (32)$$

Then the amplitude distribution function is

$$f(I) = \dot{n}_s(I) = \left(\frac{\sigma \dot{N}_o'}{2} \right) \frac{1}{I} \int_{r'} \frac{n(r') dr'}{\sqrt{\ln \left(\frac{I_o \sigma(r')}{I} \right)}} \quad (33)$$

Limits of Integration. The limits of integration are defined as follows:

It is assumed that particle radius r is less than beam radius R_B . Hence the upper limit is R_B .

The lower limit is the smallest value, r^* , of r that, when present at the point of brightest irradiance, the center of focal volume $x = x_o$, yields the amplitude I . Hence, $I = I_o \sigma(r^*)$, and

$$f(I) = \dot{n}_s(I) = \left(\frac{\delta \dot{N}_o'(t)}{2} \right) \frac{1}{I} \int_{r^*}^{R_B} \frac{n(r') dr'}{\sqrt{\ln \left(\frac{I_o \sigma(r')}{I} \right)}} \quad (34)$$

CASE 2: THE INTENSITY VARIATION AT THE FOCUS IS A DISPERSION CURVE:

$$I_f(x) = \frac{I_o}{\left[1 + \frac{(x-x_o)^2}{\delta^2} \right]^{1/2}} \quad .$$

For such a case (Fig. 14b) the amplitude distribution function is obtained in a manner similar to the one described earlier.

The scattered intensity is given by

$$I(r, x) = I_f(x) \sigma(r) = \frac{I_o \sigma(r)}{\left[1 + \left(\frac{x - x_o}{\delta}\right)^2\right]^{1/2}}, \quad (35)$$

so that

$$x = x_o + \delta^{1/2} \left[\left(\frac{I_o \sigma(r)}{I} \right)^2 - 1 \right]^{1/2}, \quad (36)$$

$$\frac{dx}{dI} = \frac{\delta^{1/2} \left[\frac{I_o \sigma(r)}{I} \right]^2}{I^3 \left[\frac{I_o \sigma(r)}{I} - 1 \right]^{1/2}} \quad (37)$$

and

$$\dot{I}(I) \equiv \dot{n}_s(I) = \dot{N}'_o(t) \int_{r^*}^{R_B} n(r') dr' \frac{dx'}{dI}. \quad (38)$$

where

$$I = I_o \sigma(r^*) .$$

Therefore

$$f(I) \equiv \dot{n}_s(I) = \frac{\dot{N}'_0 \delta^{\frac{1}{2}} I_0^2}{I^3} \int_{r^*}^{R_B} \frac{n(r') dr' [\sigma(r')]^2}{\left[\frac{I_0 \sigma(r)}{I} - 1 \right]^{1/2}} \quad (39)$$

The Inversion Problem

The equations relating $f(I)$ and $n(r)$ in the two cases are (G for Gaussion, D for dispersion curve):

$$f_G(I) \equiv \dot{n}_s(I) = \frac{\dot{N}'_0}{2I} \int_{r^*}^{R_B} \frac{n(r') dr'}{\left[\ln \left(\frac{I_0 \sigma(r)}{I} \right) \right]^{1/2}} \quad (40)$$

and

$$f_D(I) \equiv \dot{n}_s(I) = \frac{\delta^{\frac{1}{2}} \dot{N}'_0 I_0^2}{I^3} \int_{r^*}^{R_B} \frac{n(r') dr' [\sigma(r')]^2}{\left[\left(\frac{I_0 \sigma(r')}{I} \right)^2 - 1 \right]^{1/2}} \quad (41)$$

There are two methods for inverting the equations to obtain $n(r)$ from $f(I)$: (1) the general numerical method; and (2) the analytical method, based on certain simplifying approximations which render the inversion tractable. These are discussed as follows:

THE NUMERICAL SOLUTION

Let $R_B \rightarrow \infty$ and r^* is obtained from $I = I_0 \sigma(r^*)$. The amplitude distribution function in both cases [equation (40) and (41)] is of the general form,

$$\begin{aligned}
 F(I) &= \int_{g(I)}^{\infty} K(I, r) n(r) dr \\
 &= \int_0^{\infty} S[r - g(I)] K(I, r) n(r) dr \\
 &= \int_0^{\infty} K'(I, r) n(r) dr, \quad (42)
 \end{aligned}$$

where S is a step function.

The quantities are defined as:

$$I_j = I_0 + j \Delta I,$$

$$r_i = r_0 + i \Delta r.$$

For simplicity let $r_0 = 0$, $I_0 = 0$, then

$$I_j = j \Delta I ,$$

and

$$r_i = i \Delta r ,$$

so that

$$\begin{aligned} F(I_j) &= \sum_{i=0}^{i_{\max}} \Delta r K(j\Delta I, i\Delta r) n(i\Delta r) \\ &= \sum_{i=0}^{i_{\max}} K_{ji} n(i\Delta r) , \end{aligned} \tag{43}$$

or,

$$\begin{aligned} F_j &= \sum_{i=0}^{i_{\max}} K_{ji} n_i \\ \vec{F} &= \mathbf{K} \cdot \vec{n} , \end{aligned} \tag{44}$$

where \mathbf{K} is a matrix, so that

$$\vec{n} = \mathbf{K}^{-1} \cdot \vec{F} .$$

It is possible to set up a computation scheme for such a matrix inversion problem and then obtain a histogram for $n(r)$ versus r . The shape of the $n(r)$ curve will depend on the choice of the values of the intervals ΔI and Δr and the total number of points j and i . At least a thousand pulses should be taken into account for sufficient accuracy.

ANALYTICAL SOLUTION

Let us assume that $R_B \gg r$, so that $R_B \rightarrow \infty$; and that, the particles are large compared to λ of the incident light, so that

$$Q(x) \simeq 2 \text{ and } \sigma(r) \simeq 2\pi r^2 .$$

Then the equations reduce to

$$f_G(I) = \frac{\delta \dot{N}_0}{2I} \int_{r^*}^{\infty} \frac{n(r') dr'}{[\ln A r^2]^{1/2}} \quad (45)$$

and

$$f_D(I) = \frac{4\pi^2 \delta^{\frac{1}{2}} \dot{N}_0' I_0^2}{I^3} \int_{r^*}^{\infty} \frac{n(r') dr' (r')^4}{[(Ar^2)^2 - 1]^{1/2}} , \quad (46)$$

where

$$A = \frac{2\pi I_0}{I} .$$

Choosing Junge's simple power-law model for $n(r)$, namely,

$$n(r) = C_0 r^{-\nu} \text{ [cm}^{-4}\text{]} ,$$

the above equations become

$$f_G(I) = \frac{C_0 \delta N'_0}{2 I} \int_{r^*}^{\infty} \frac{r^{-\nu} dr}{(\ln A r^2)^{1/2}} \quad (47)$$

and

$$f_D(I) = \frac{4\pi^2 \delta^{\frac{1}{2}} N'_0 C_0 I_o^2}{I^3} \int_{r^*}^{\infty} \frac{r^{(4-\nu)} dr}{[(Ar^2) - 1]^{1/2}} , \quad (48)$$

where

$$r^* = \frac{1}{\sqrt{A}} , \quad A = \frac{2\pi I_o}{I} .$$

Introducing the variable (t) ,

$$t = Ar^2 .$$

Then,

$$f_G(I) = \frac{C_o \delta N_o' (2\pi I_o)^{\frac{\nu+1}{2}}}{2 I^{\frac{\nu+1}{2}}} \int_1^{\infty} \frac{t^{-\frac{\nu+1}{2}} dt}{\sqrt{\ln t}} \quad (49)$$

and

$$f_D(I) = \frac{4\pi^2 C_o \delta^{\frac{1}{2}} N_o' (2\pi I_o)^{\frac{5-\nu}{2}}}{I^{\frac{\nu+1}{2}}} \int_1^{\infty} \frac{t^{\frac{3-\nu}{2}} dt}{\sqrt{t^2 - 1}} \quad (50)$$

The Gaussian Case .

$$\text{Let } \frac{1}{Z} = t \quad .$$

Then,

$$f_G(I) = \frac{C_o \delta N_o'}{2} \left(\frac{2\pi I_o}{I} \right)^{\frac{\nu+1}{2}} \int_0^1 \frac{Z^{\frac{\nu-3}{2}} dZ}{\sqrt{\ln \frac{1}{Z}}} \quad (51)$$

From the tables of Integrals

$$\int_0^1 \frac{x^m dx}{\sqrt{\ln \frac{1}{x}}} = \sqrt{\frac{\pi}{m+1}} \quad , \quad m > -1 \quad ,$$

we obtain

$$\begin{aligned}
 f_G(I) \equiv \dot{n}_s(I) &= \frac{\delta \dot{N}_o' C_o}{2} \left(\frac{2\pi I_o}{I} \right)^{\frac{1+\nu}{2}} \sqrt{\frac{\pi}{\nu-1}} , \\
 &= C_G I^{-\left(\frac{1+\nu}{2}\right)} \quad \text{for } \nu > 1 .
 \end{aligned} \tag{52}$$

$$\text{Let } \sqrt{I} = i ,$$

$$\text{so that } di = -\frac{dI}{2\sqrt{I}} .$$

Then,

$$f(I) dI = - f(i) di = f(i) \frac{dI}{2\sqrt{I}} , \tag{53}$$

$$\text{or, } f(i) = 2\sqrt{I} f(I)$$

$$= 2 C_G I^{-\left(\frac{1+\nu}{2}\right)} I^{\frac{1}{2}}$$

$$= 2 C_G I^{-\frac{\nu}{2}}$$

$$= 2 C_G i^{-\nu} . \tag{54}$$

Thus, for a Gaussian intensity distribution at the focus, if the model for

$$n(r) = C_o r^{-\nu} ,$$

then the amplitude distribution function also has the same power law,

$$f(i) = (C'_G) i^{-\nu} .$$

Hence, a log-log plot of $\dot{n}_s(i)$ versus i yields the value of ν for the size-distribution $n(r)$.

The Dispersion Case:

The integral in the equation can be solved for a power-law model of $n(r)$ only for the cases when

$$\nu = 5, 7 ,$$

Such a power law for $n(r)$ occurs in nature only at special locations or altitudes. In these cases

$$f_D(I) \propto I^{-\frac{1+\nu}{2}} ,$$

and again,

$$f_D(i) = \dot{n}_{SD}(i) \propto i^{-\nu} . \quad (55)$$

The log-log plot of $\dot{n}_{SD}(i)$ versus i , yields the value of ν .

Experimental Results

On the same samples of Al_2O_3 settling in air, both the photographic and laser scattering methods were used simultaneously to measure their size-distributions. The results of the size-distribution as obtained by the photographic method¹ are given in Figure 10. From the chart-recorder tape were measured the heights of the signal due to scattered light, and the number of pulses for each of the various ranges of signal amplitude was counted. These values were plotted (Fig. 16a).

The slope of the curve yields the value of $(\nu/2) = 1.7$, so that $\nu \approx 3.4$, which is close to the value as obtained in Figure 10 for the same sample of Al_2O_3 particles.

Also, similar results are shown in Figure 16b for ambient air drawn through the focal region. They provide a ν of approximately 3.2.

THE DUAL-BEAM VELOCIMETER

The Theoretical Analysis

As mentioned earlier, in the velocimeter mode the cylindrical lens is replaced by a system composed of a beam splitter (50 percent reflectivity), a plane front-surface mirror, and a convex lens (Fig. 11). The original beam is split into two parallel beams of nearly equal intensity and focused at the same point as the original in the sizer mode. At the crossover region of the two beams, a pattern of interference fringes is formed (Figs. 17, 18, 19). The number of fringes is greater for larger angular separation (θ) of the beams. However, to block off the direct beams by the dark spot (diameter 0.63 cm) in front of the collecting lens, the separation distance between the two beams at the spot is kept to within 0.5 cm. All the other components of the entire optical system remain undisturbed.

When a particle traverses the system of planar fringes it gives a modulation of the scattered light at a frequency proportional to the velocity component perpendicular to the plane of the fringes.

It may be seen as a method of placing at the focal volume a precise linear scale (of planar fringes) which is used to measure the velocity of the traversing particles through the focal volume.

A very high degree of spatial resolution can be achieved by electronically filtering out the signals from particles which are not quite passing through the focal volume of the beams. This way the rate of passage of particles per unit volume of the space can be accurately calculated. This yields the number concentration (cm^{-3}) of the aerosols per unit time.

It should be noted that in principle, if the intensity distribution of the fringe system is known, it is then possible to determine the size of the particle from the amplitude of the signal.

In this paper only the velocity measurement aspect of this mode of operation will be presented. The simultaneous sizing of the particles will be left for a later publication.

The velocity component of the particles can be obtained also in terms of the Doppler beat frequency. Whether one analyzes this velocimeter in terms of fringes (real or virtual) or in terms of the Doppler frequency shifts, the velocity component measured is the same. The two points of view are equal. The fringe method treatment is presented as follows:

It is shown in equation (2), that the width of the beam at the focal waist is (Fig. 17a)

$$\delta = \lambda f / D_B \quad . \quad (56)$$

Thus, the depth of field is

$$l_1 = \frac{f}{D_B} \frac{\delta}{\lambda} = \lambda \left(\frac{f}{D_B} \right)^2 \quad . \quad (57)$$

BEAM CROSSOVER REGION

If the axial length of the crossover region is l_2 at 1/2-intensity points (Fig. 17c), then for small angular separation $\theta = \frac{D}{f}$ and $l_1 \gg l_2$, the two beams in the crossover regions have uniform diameters, so that

$$I_2 \simeq \frac{\delta}{\theta} = \frac{\lambda f^2}{2 D D_B} = \frac{D_B}{D} I_1 . \quad (58)$$

Thus, it is required that $D_B \ll D$, for this analysis.

The beams have a gaussian intensity distribution

$$I(g) = \psi_0^2 e^{-\left(2g^2/R_B^2\right)} , \quad (59)$$

or amplitude distribution

$$\psi(g) = \psi_0 e^{-\left(g^2/R_B^2\right)} , \quad (60)$$

where, by the normalization condition,

$$\psi_0 = \left(\frac{2 P_L}{\pi R_B^2} \right)^{1/2} , \quad (61)$$

where P_L is the beam power, and $R_B = \frac{1}{2} D_B$.

The amplitude distribution of the two identical beams in the $x - z$ plane at the focal region is given by superposition

$$\psi(x, z) = \psi_1(x, z) + \psi_2(x, z) , \quad (62)$$

where for the two beams, the amplitudes are

$$\psi_1(x, z) = \psi_0 \exp \left[- \frac{\left(z - \frac{\theta x}{2} \right)^2}{\left(\frac{\delta}{2} \right)^2} \right] \exp \left[i \frac{2\pi}{\lambda} \left(x + \frac{z\theta}{2} \right) \right] \quad (63)$$

and

$$\psi_2(x, z) = \psi_0 \exp \left[- \frac{\left(z + \frac{\theta x}{2} \right)^2}{\left(\frac{\delta}{2} \right)^2} \right] \exp \left[i \frac{2\pi}{\lambda} \left(x - \frac{z\theta}{2} \right) \right] \quad (64)$$

Then the intensity distribution in the crossover region is

$$\begin{aligned} I = |\psi|^2 &= |\psi_1|^2 + |\psi_2|^2 + (\psi_1 \psi_2^* + \psi_1^* \psi_2) \\ &= \psi_0^2 \exp \left[- 2 \left(z - \frac{\theta x}{2} \right)^2 / \left(\frac{\delta}{2} \right)^2 \right] \\ &+ \psi_0^2 \exp \left[- 2 \left(z + \frac{\theta x}{2} \right)^2 / \left(\frac{\delta}{2} \right)^2 \right] \\ &+ 2 \psi_0^2 \exp \left[- 2 \frac{z^2}{\left(\frac{\delta}{2} \right)^2} - \frac{\theta^2 x^2}{2 \left(\frac{\delta}{2} \right)^2} \right] \cos \left(\frac{2\pi}{\lambda} z \theta \right). \end{aligned} \quad (65)$$

For $D_B \ll D$, $\theta = D/f$, and $l_2 = \delta / \theta$.

$$I_{xz} = |\psi|^2 = \psi_0^2 e^{-2 \left(z - \frac{Dx}{2f} \right)^2 / \left(\frac{\delta}{2} \right)^2}$$

$$\begin{aligned}
& + \psi_0^2 e^{-\left(z + \frac{Dx}{2f}\right)^2 / \left(\frac{\delta}{2}\right)^2} \\
& + 2 \psi_0^2 e^{-2 \left[\frac{z^2}{\left(\frac{\delta}{2}\right)^2} + \frac{x^2}{l^2} \right]} \cos \left[\frac{2\pi D}{\lambda f} z \right] \quad . \quad (66)
\end{aligned}$$

For a cylindrical lens, the fringe intensity distribution in the z-x plane is given by equation (66) and in the z-y plane by

$$I_{zy} = (\psi_0)^2 e^{-2 \left(\frac{x}{R_B} \right)^2} \quad (67)$$

so that the shape of the crossover region in 3-dimensions looks like Figure 20.

If v is a component of velocity of the particle perpendicular to the fringes, then time taken to traverse a width δ of the beam is

$$t = \frac{\delta}{v} = \frac{\lambda f}{D_B v} \quad , \quad (68)$$

yielding a frequency shift of

$$\Delta f = \frac{1}{t} = \frac{D_B v}{\lambda L} \quad . \quad (69)$$

The focal region is crossed by planar fringes separated by a spacing (Figs. 17, 18, 19)

$$a = \frac{\lambda}{2 D \sin \theta}$$

$$\simeq \frac{\lambda}{2 \theta D} \quad (\text{for small } \theta) \quad . \quad (70)$$

The frequency of modulation of scattered light as the particle traverses the fringes is

$$\bar{f} = \frac{v}{a} = \frac{vD}{\lambda f} \quad , \quad (71)$$

where fringe spacing

$$a = \frac{\lambda f}{D} \quad . \quad (72)$$

Hence, the ratio of the frequency spread because of transit through the beam to the frequency of modulation is (Fig. 21)

$$\frac{\Delta f}{f} = -\frac{D_B}{D} \quad . \quad (73)$$

The peak A corresponds to the averaging out of the first two terms in expression I, while the peak B is due to the interference (third) term.

We can eliminate the spectrum A by frequency filtering and restrict the axial response to a length $\sim 2\delta_2$ of the crossover region.

THE PULSE AVERAGING

The number of fringes is $N = \frac{D}{D_B}$.

If I_0 is the intensity at the center of the pulse, then time integration yields

$$\int I dt + \frac{1}{v} \int I dz = \frac{\lambda D_B}{vf} e^{-C_1 \left[\frac{Z D D_B}{\lambda f^2} \right]^2} e^{-C_1 \left[\frac{x}{D_B} \right]^2} e^{-\left[\frac{f - f}{\Delta f} \right]^2}.$$

(74)

CONCLUSIONS

The instrument was designed and built at Wayne State University, Detroit, Michigan, during the author's stay, and successfully tested for its performance. The results were quite gratifying considering that this was a first generation instrument which was built with easily accessible economy-priced equipment.

It provides a technical know-how for building a much more sophisticated and versatile instrument within a relatively short period of time and a modest sum of money. The problems and bugs encountered were successfully solved along the way.

Extensive tests with different size samples of Al_2O_3 particles were performed using the two parts of the instrument separately as well as operating them in conjunction. Results of one such simultaneous measurement of the diameter Al_2O_3 particles show a good agreement for the size-distribution $n(r)$ (Figs. 11 and 16b) as obtained by the photographic and the laser scattering methods.

The experiments with the LSC used in the velocimeter mode have not been given here, and will be reported subsequently.

Thus we see that the instrument is capable of providing a standard source of particles whose size-distribution and velocity (or velocity-distribution) are known. The knowledge of these two aspects of aerosols are essential for a successful calibration of the continuous wave CO_2 - laser Doppler Systems at Marshall Space Flight Center.

The photographic system has been subsequently used successfully in the measurement of the size-distribution of artificial fogs. The instrument can be used for measuring the same physical properties of particles in colloidal solutions, since the glass-cell is water-tight when closed.

The feasibility of doing photographic studies on vortex formations in water and acoustic coagulation of aerosols has also been successfully demonstrated, but the work will be reported at a future date.

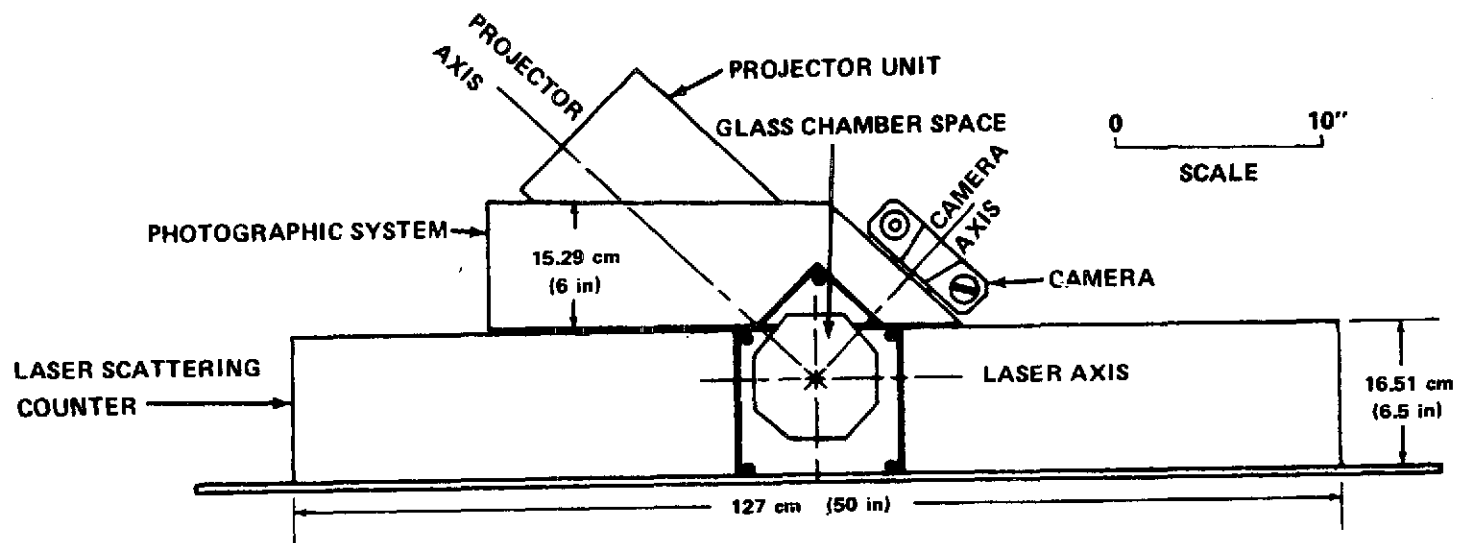


Figure 1a. Plan of the sizer-velocimeter.

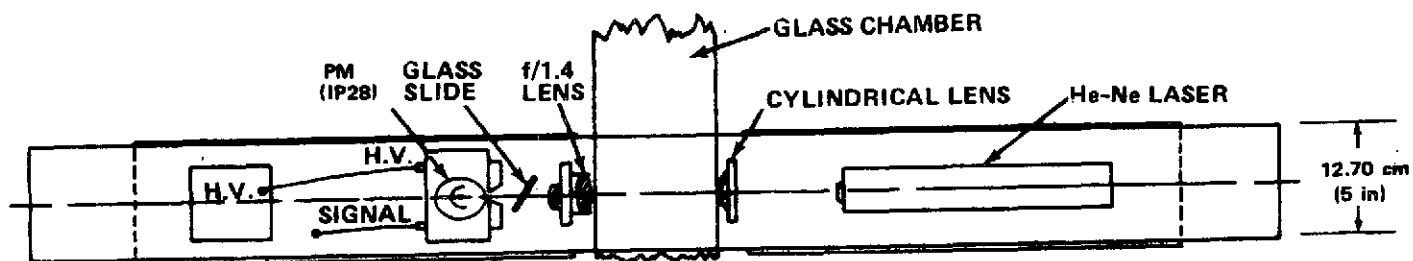


Figure 1b. Side view of the laser scattering counter (LSC).

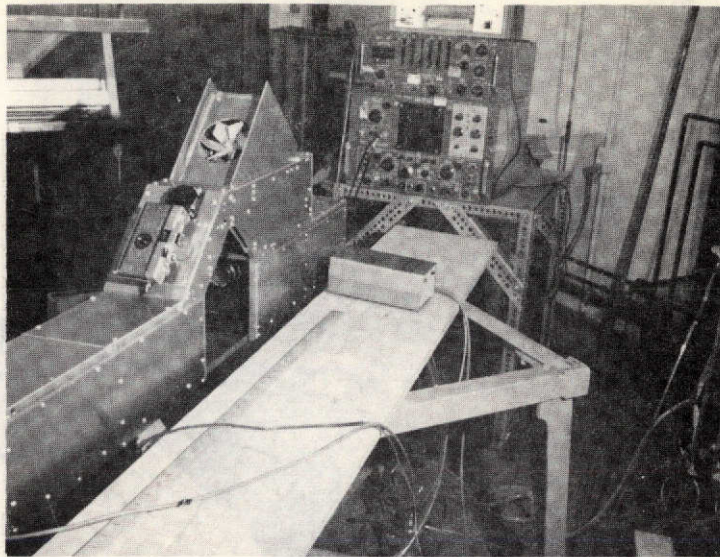
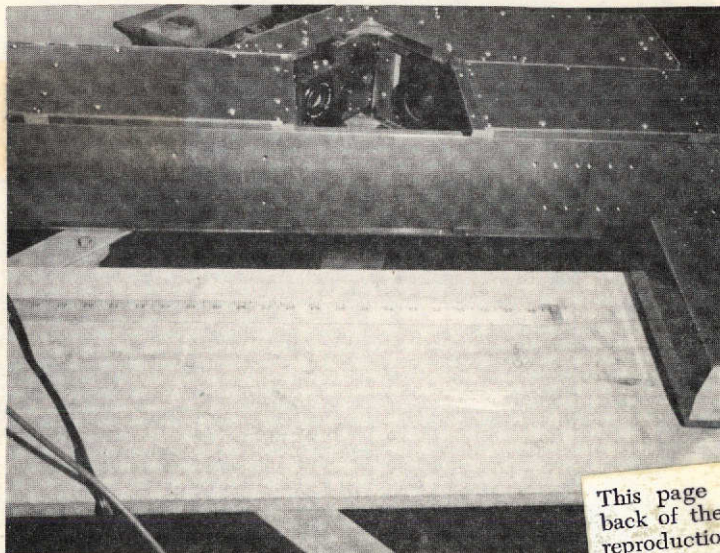


Figure 2a. The photographic system and the LSC fitted together for simultaneous operation



This page is reproduced at the back of the report by a different reproduction method to provide better detail.

Figure 2b. Details of the photographic system when used in conjunction with the LSC.

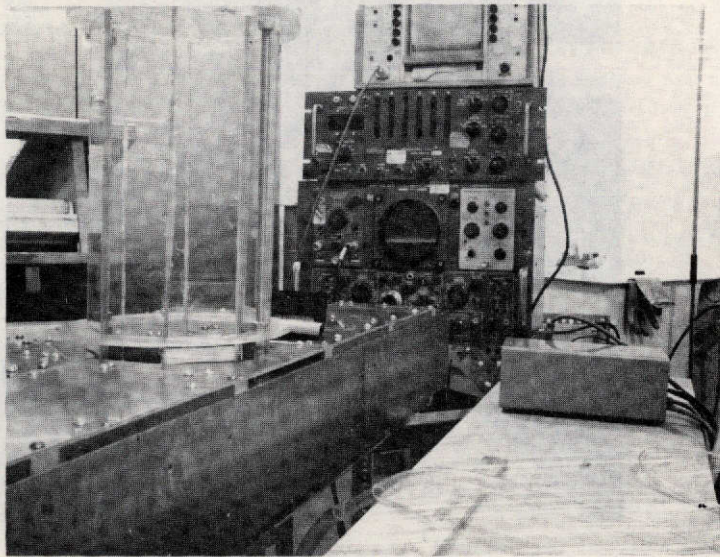


Figure 2c. Glass chamber fitted for simultaneous operation of the photographic system and the LSC.

This page is reproduced at the back of the report by a different reproduction method to provide better detail.

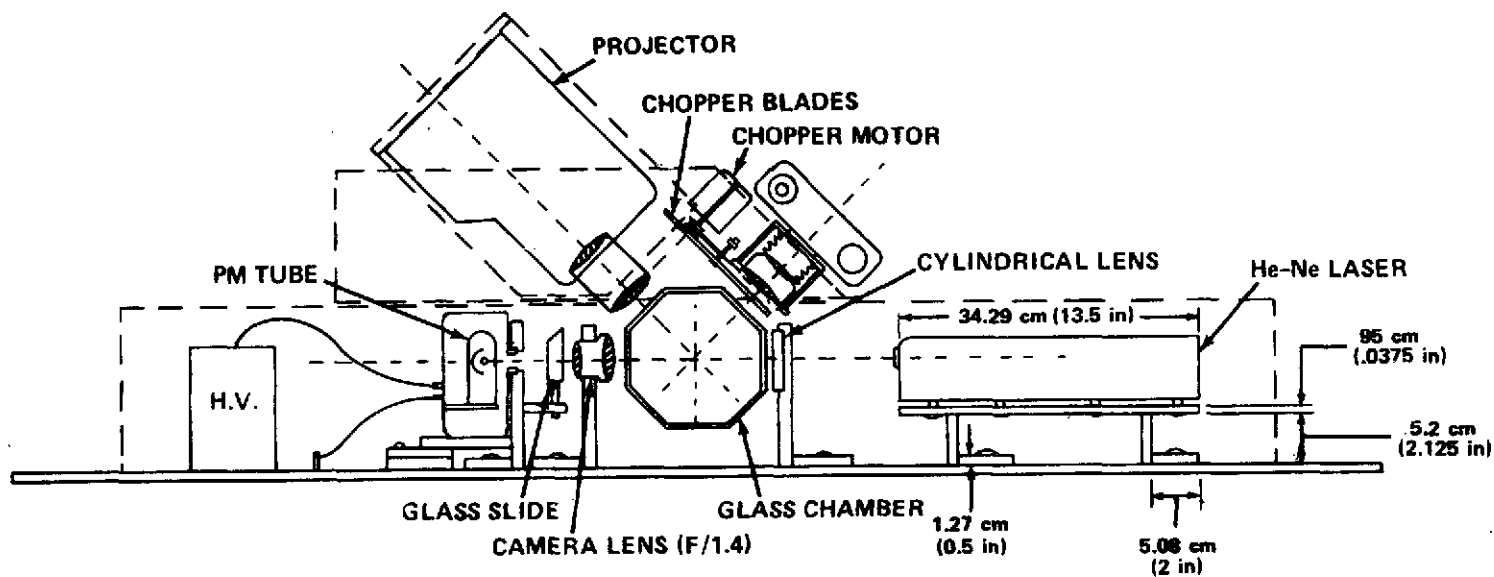


Figure 3. Plan of the instrumentation.

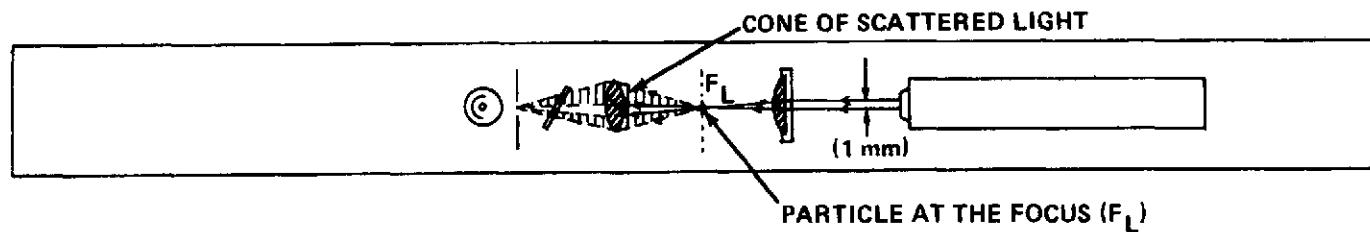


Figure 4. Schematic diagram of the LSC optics.

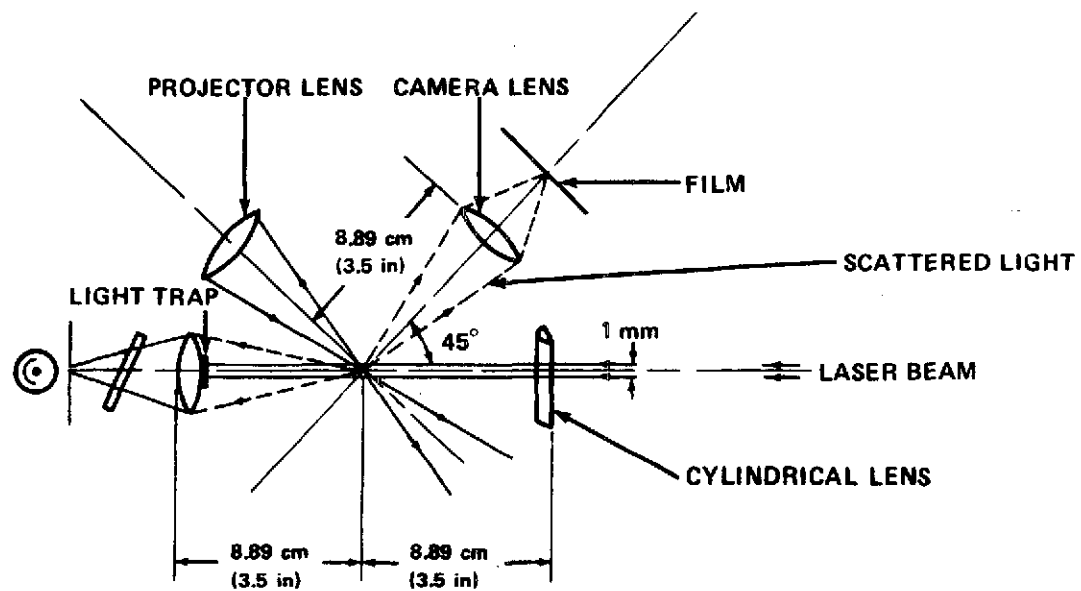


Figure 5. Optical schematic of the LSC and photographic system used in conjunction.

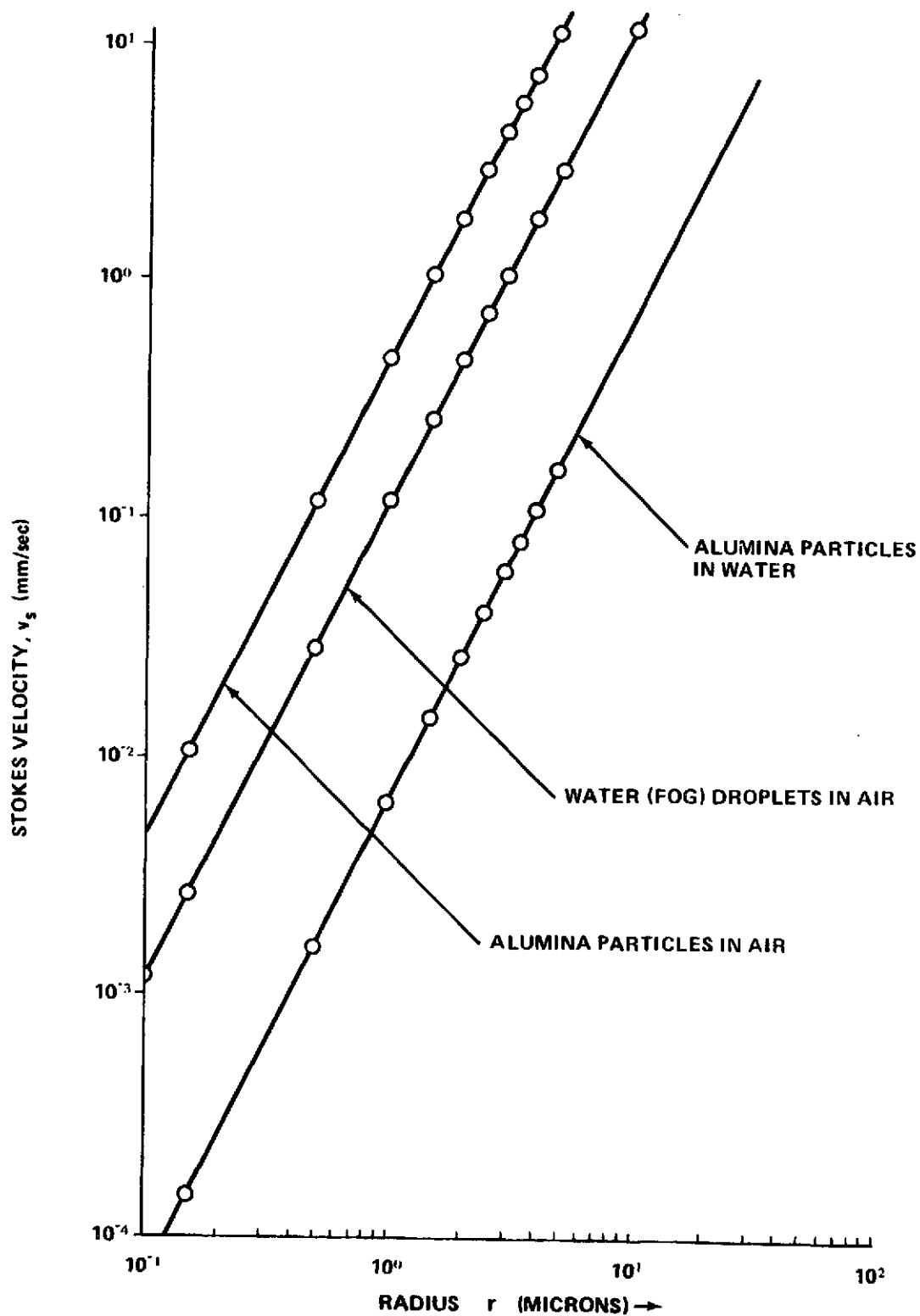


Figure 6. Stokes' velocity versus radius.

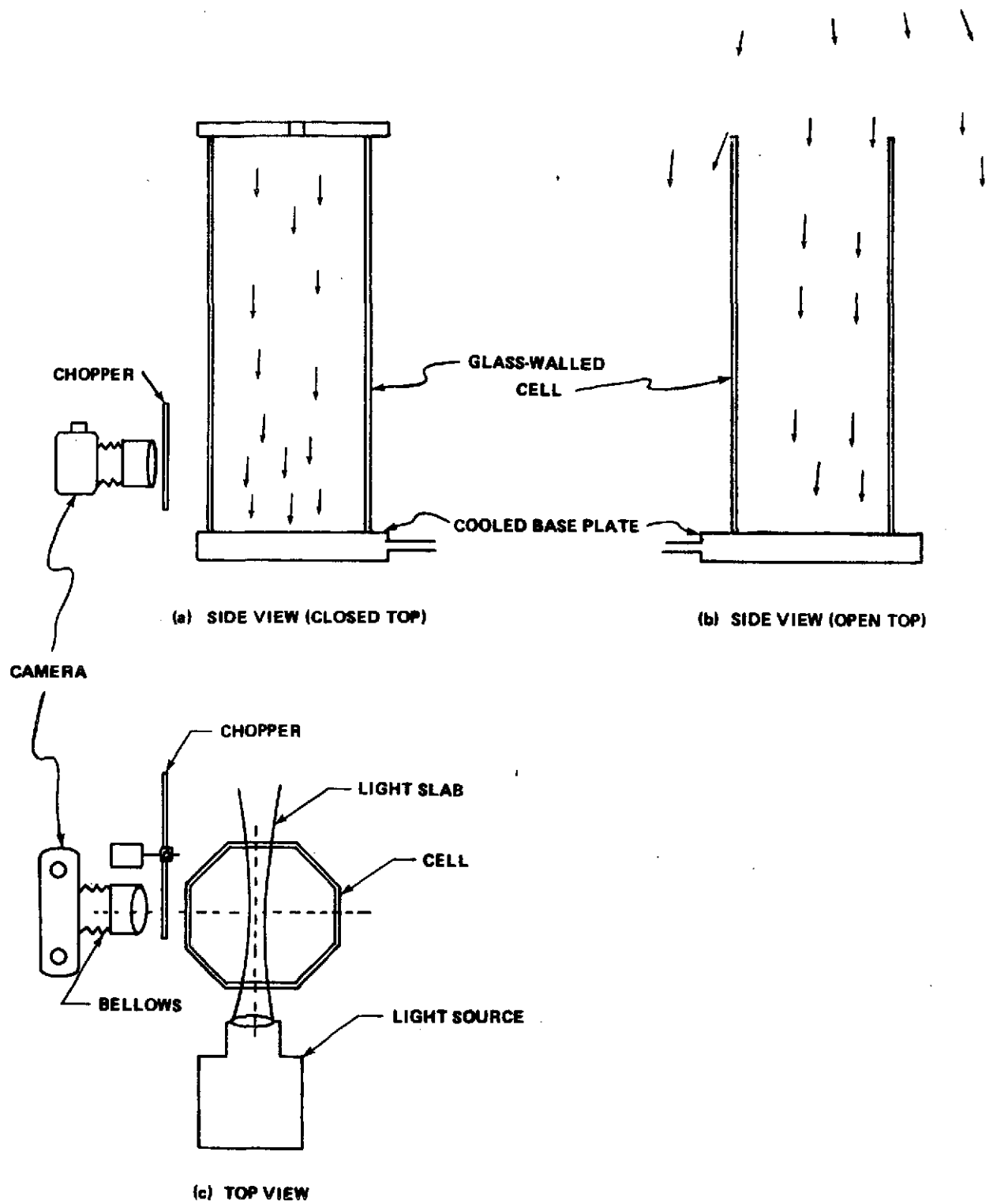


Figure 7. Schematic illustration of the method.

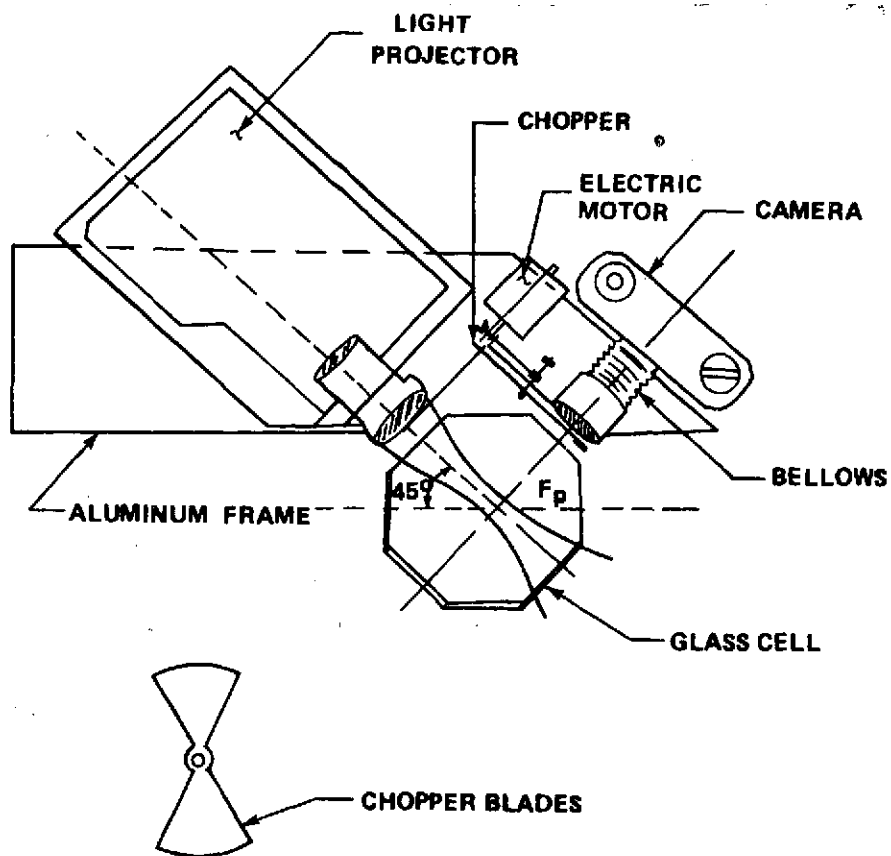


Figure 8. Schematic diagram of the photographic system.

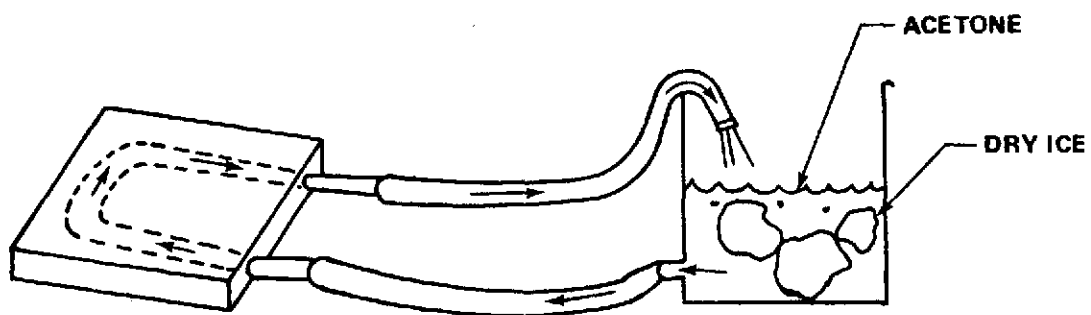


Figure 9. Acetone and dry ice pump.

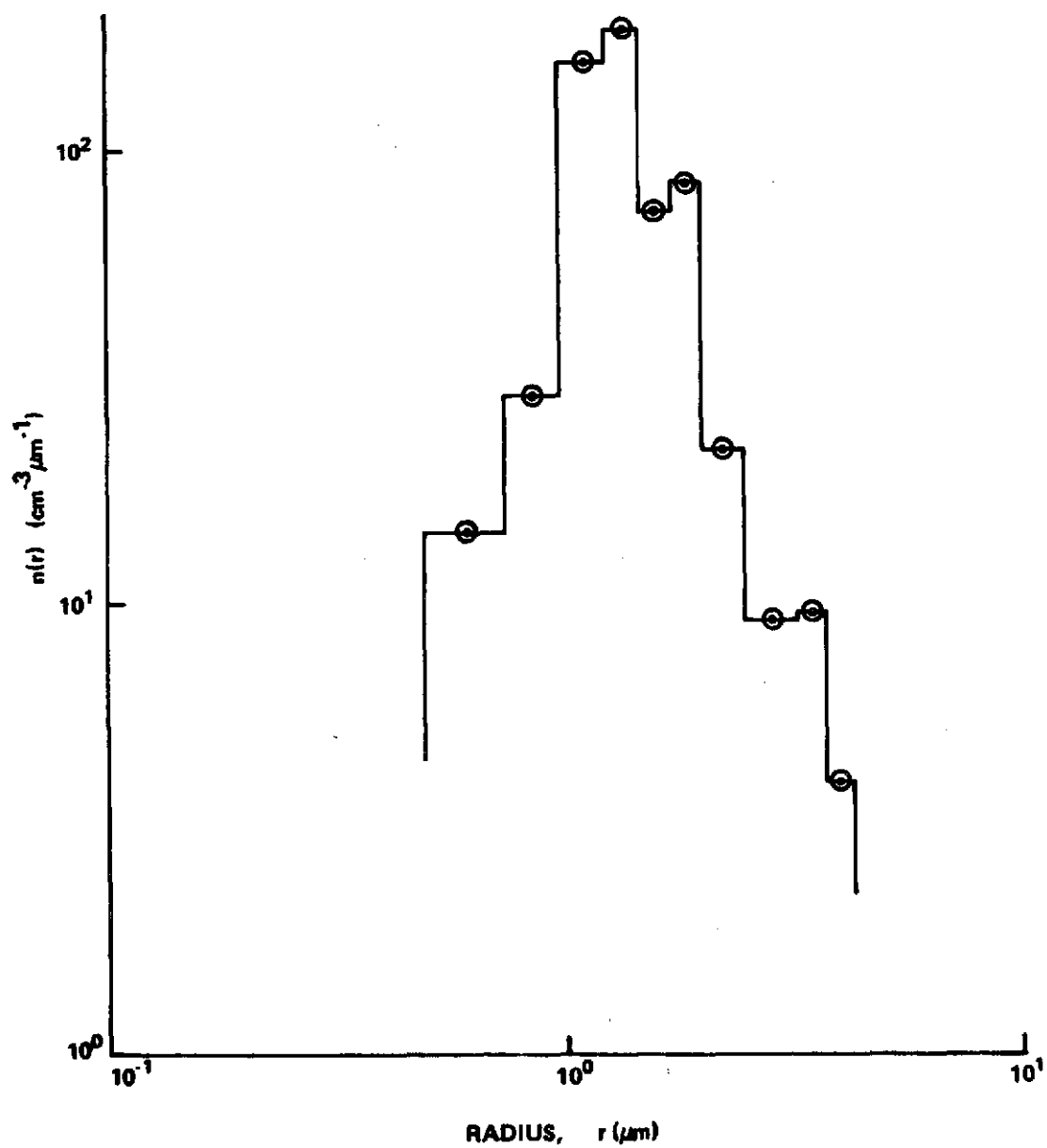


Figure 10. Graph of $n(r)$ versus r for Al_2O_3 particles of (supplier quoted) radius of 1.5 microns.

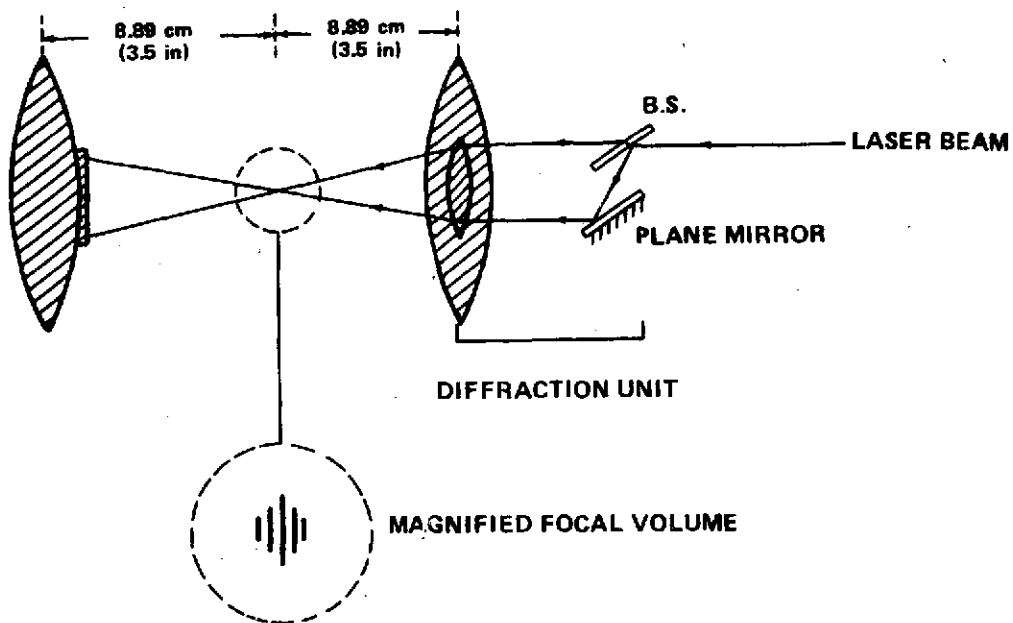


Figure 11. LSC used as a fringe-system counter.

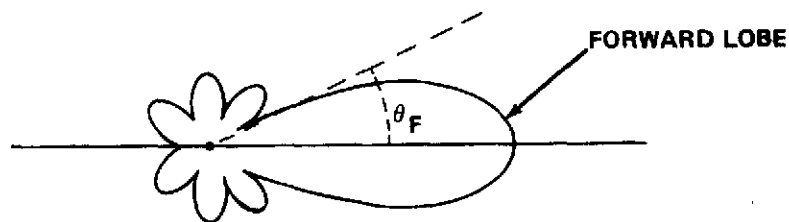


Figure 12. Polar diagram of the light scattered by a Mie-particle.

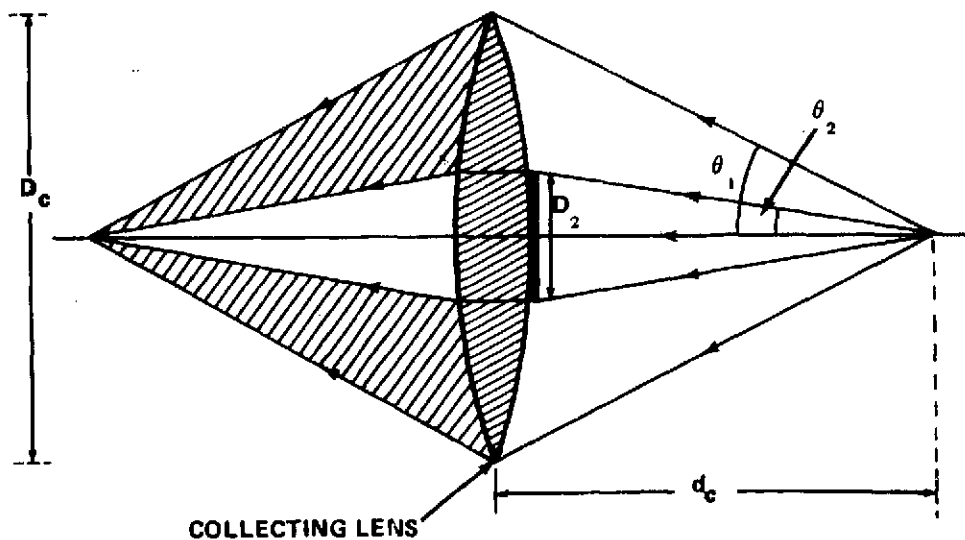


Figure 13. Schematic diagram of the LSC collecting lens.

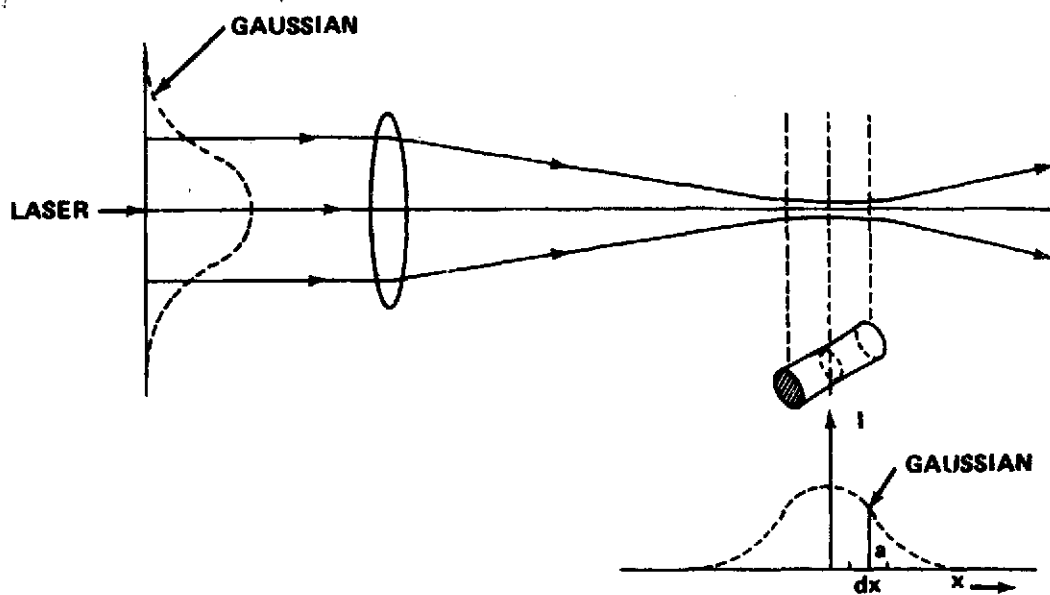


Figure 14a. Schematic of the intensity distribution at the focal volume for a spherical focusing lens.

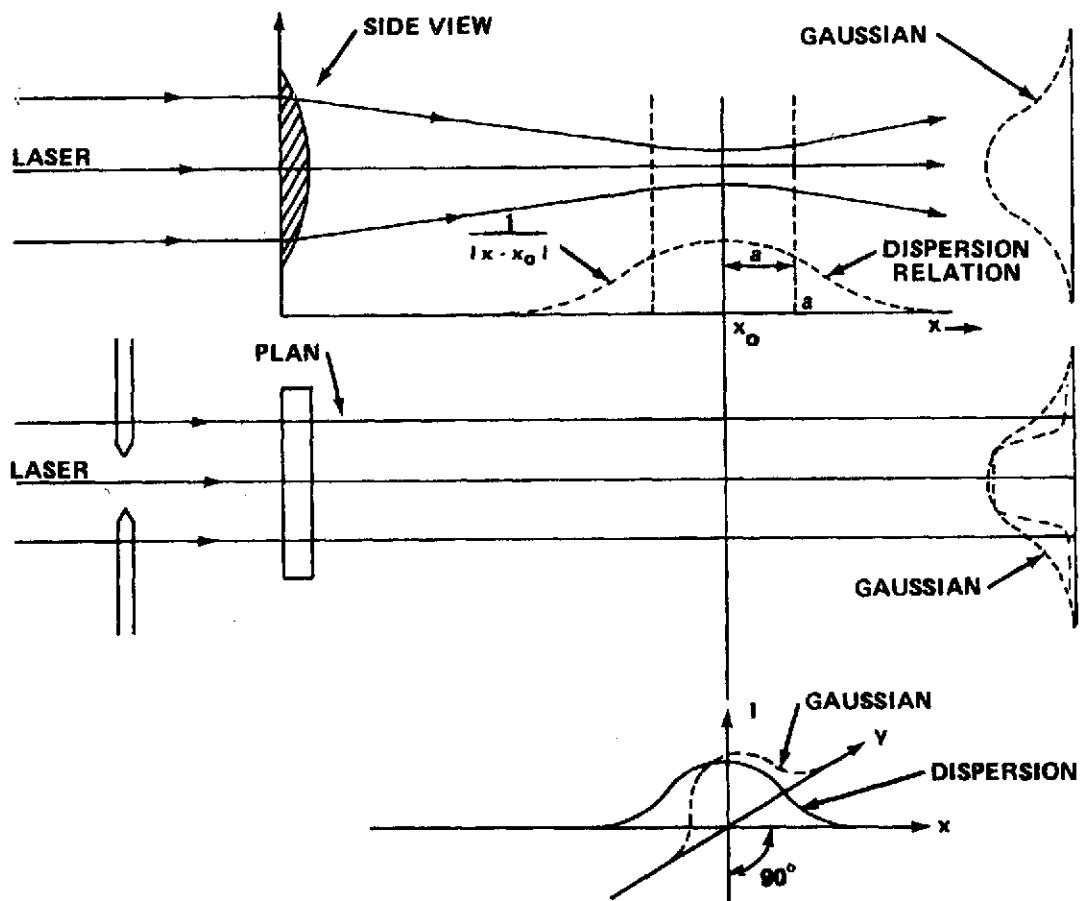


Figure 14b. Schematic of the intensity distribution at the focal volume for a cylindrical focusing lens.

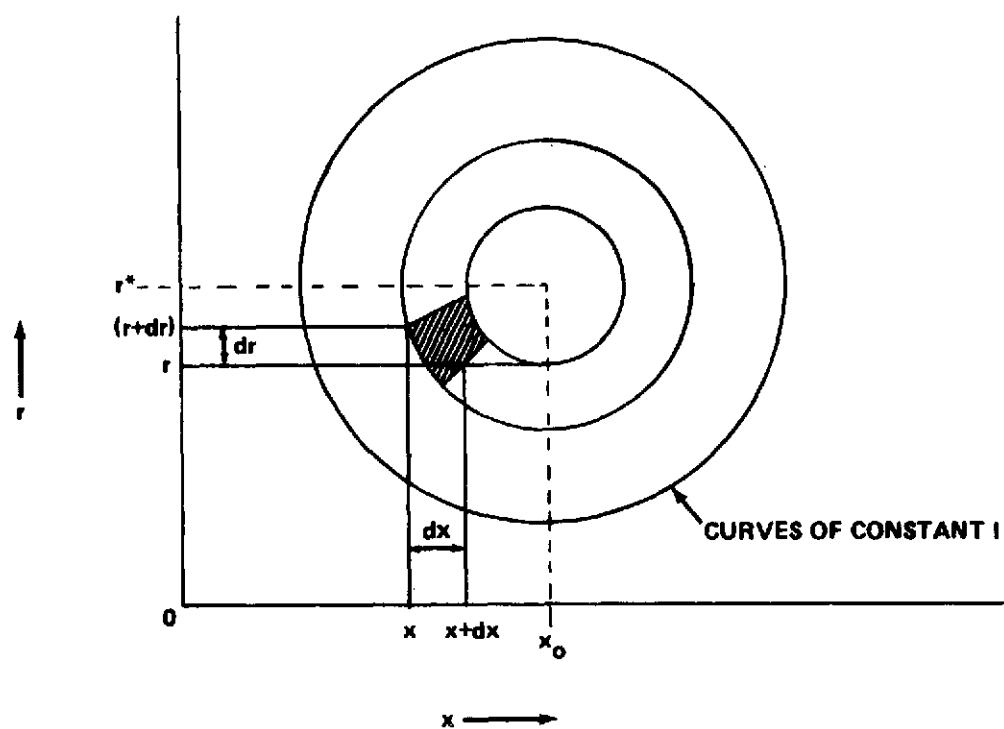


Figure 15. Contours of constant intensity as a function of x and r .

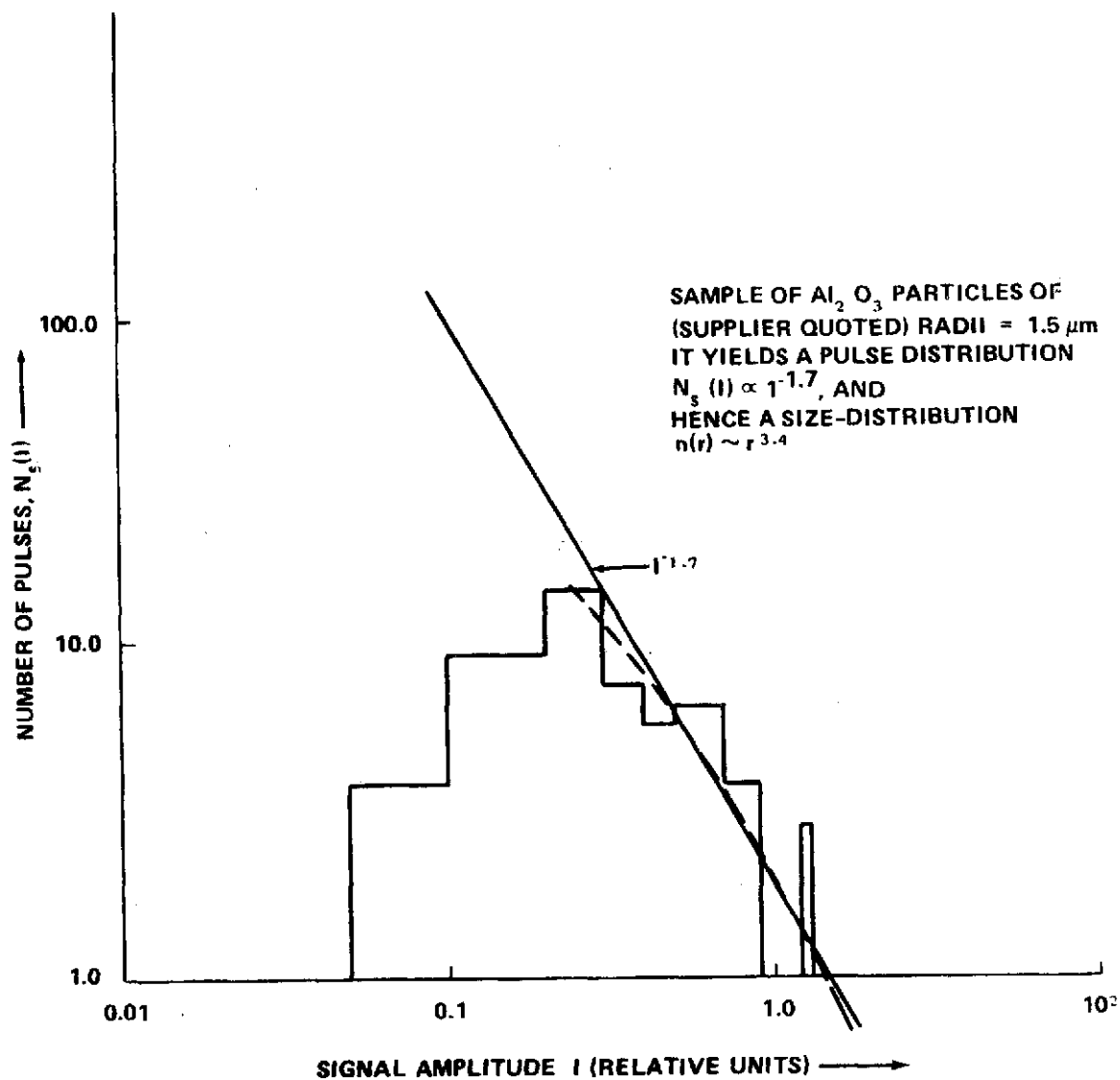


Figure 16a. Graph of $N_s(I)$ versus I for the Al_2O_3 particles of 1.5 microns radius.

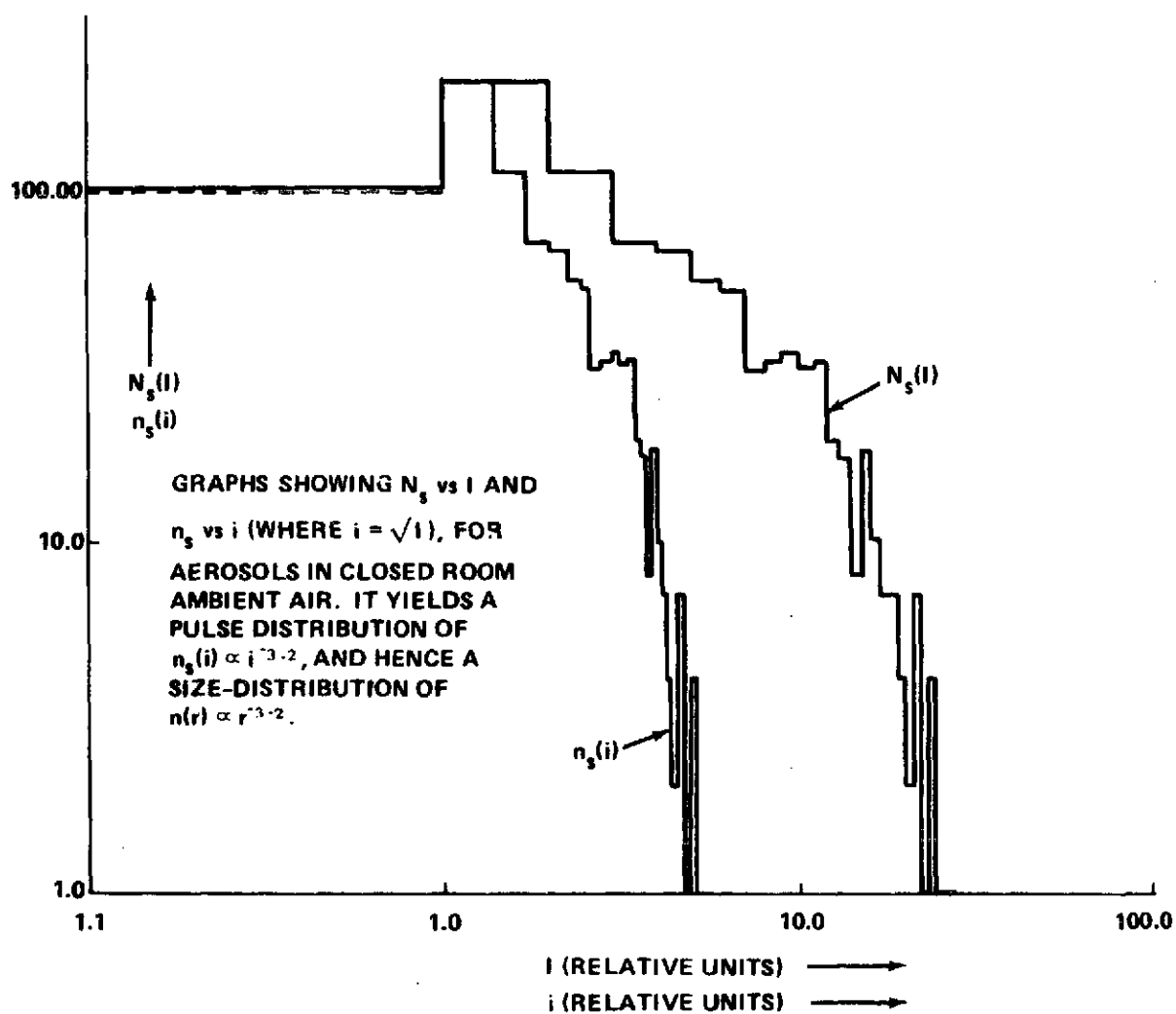


Figure 16b. Graphs of N_s versus I and n_s versus i ($i = \sqrt{I}$) for aerosols in closed room ambient air.

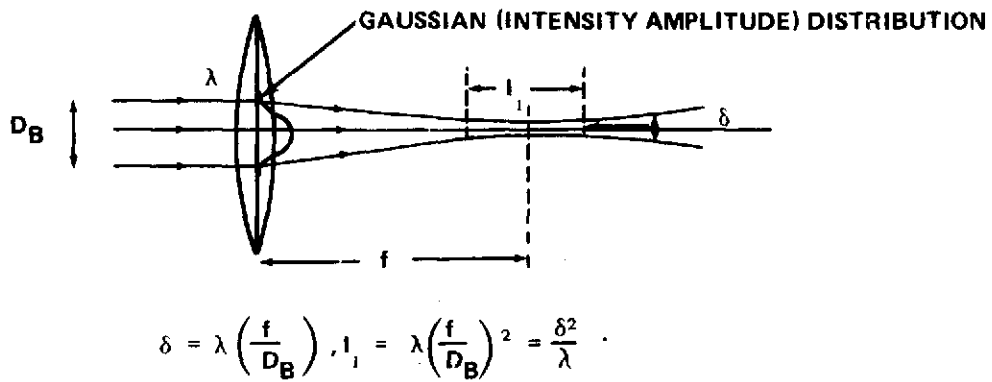


Figure 17a. Focal volume dimensions.

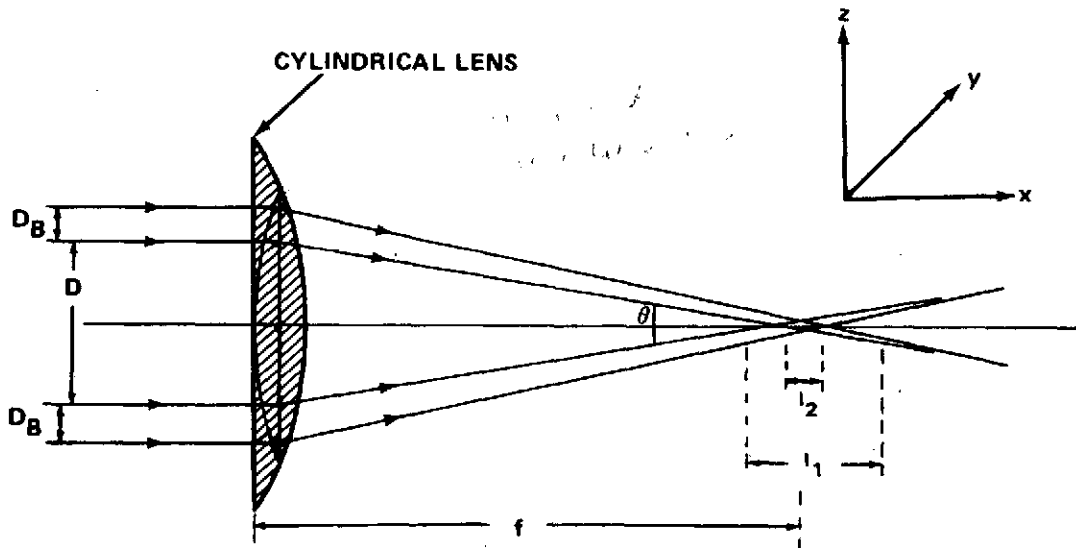


Figure 17b. Two-beam diffraction pattern at the focus.

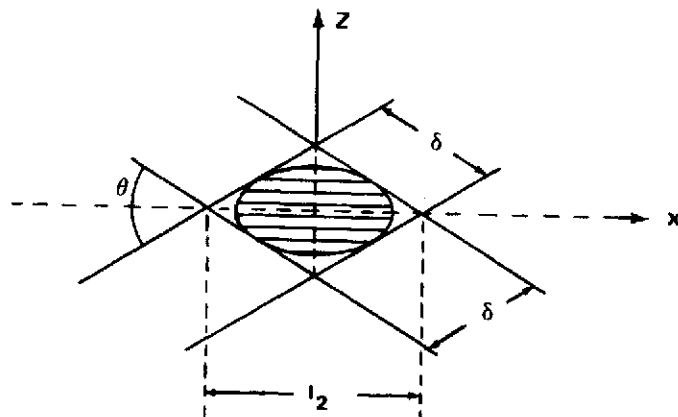


Figure 17c. The beam crossover region, where $\theta = \frac{D}{f}$.

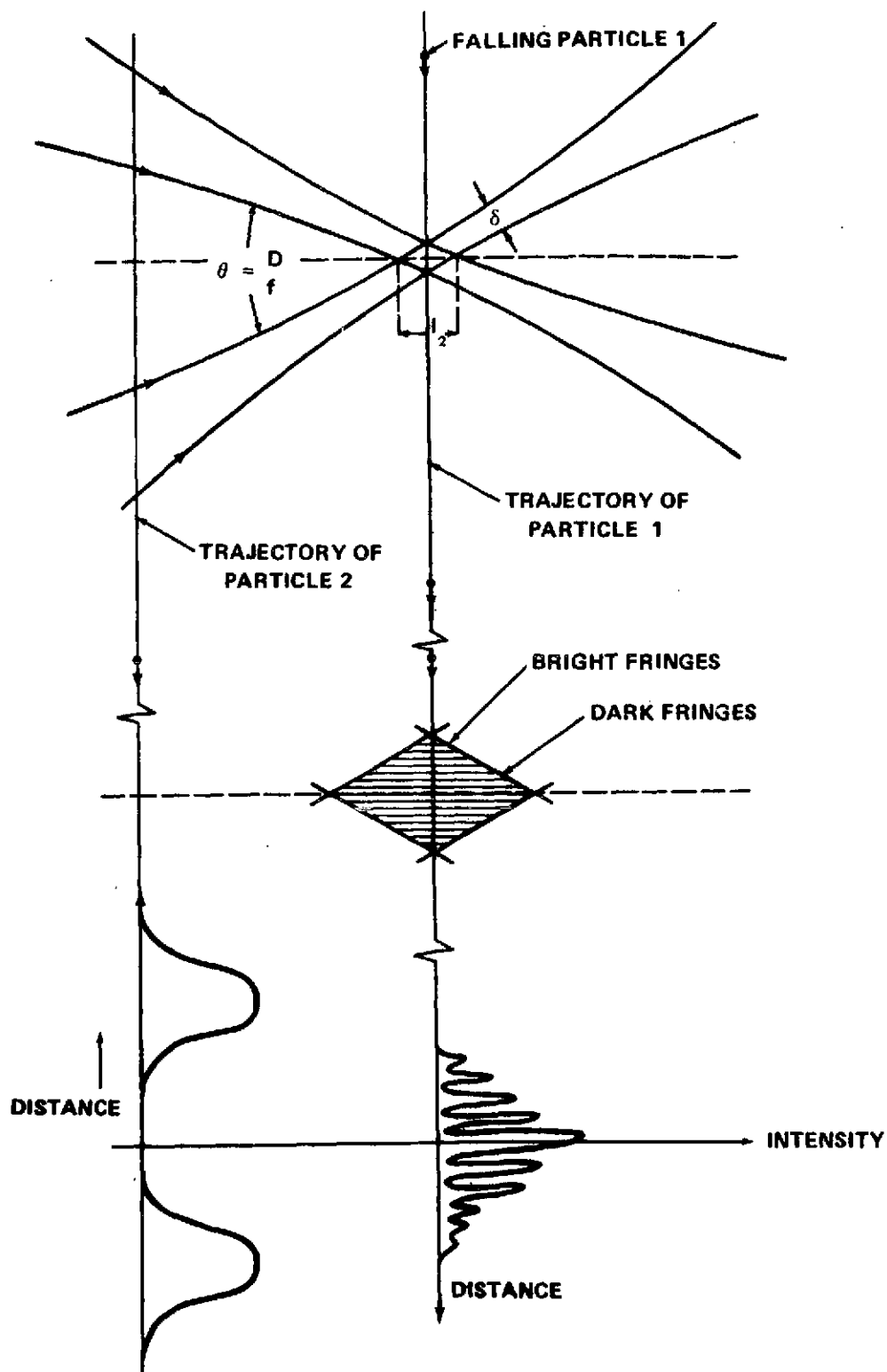


Figure 18. Schematic of intensity patterns for the trajectories of two particles: particle 1 through the focal volume; particle 2 through the non-focal region.

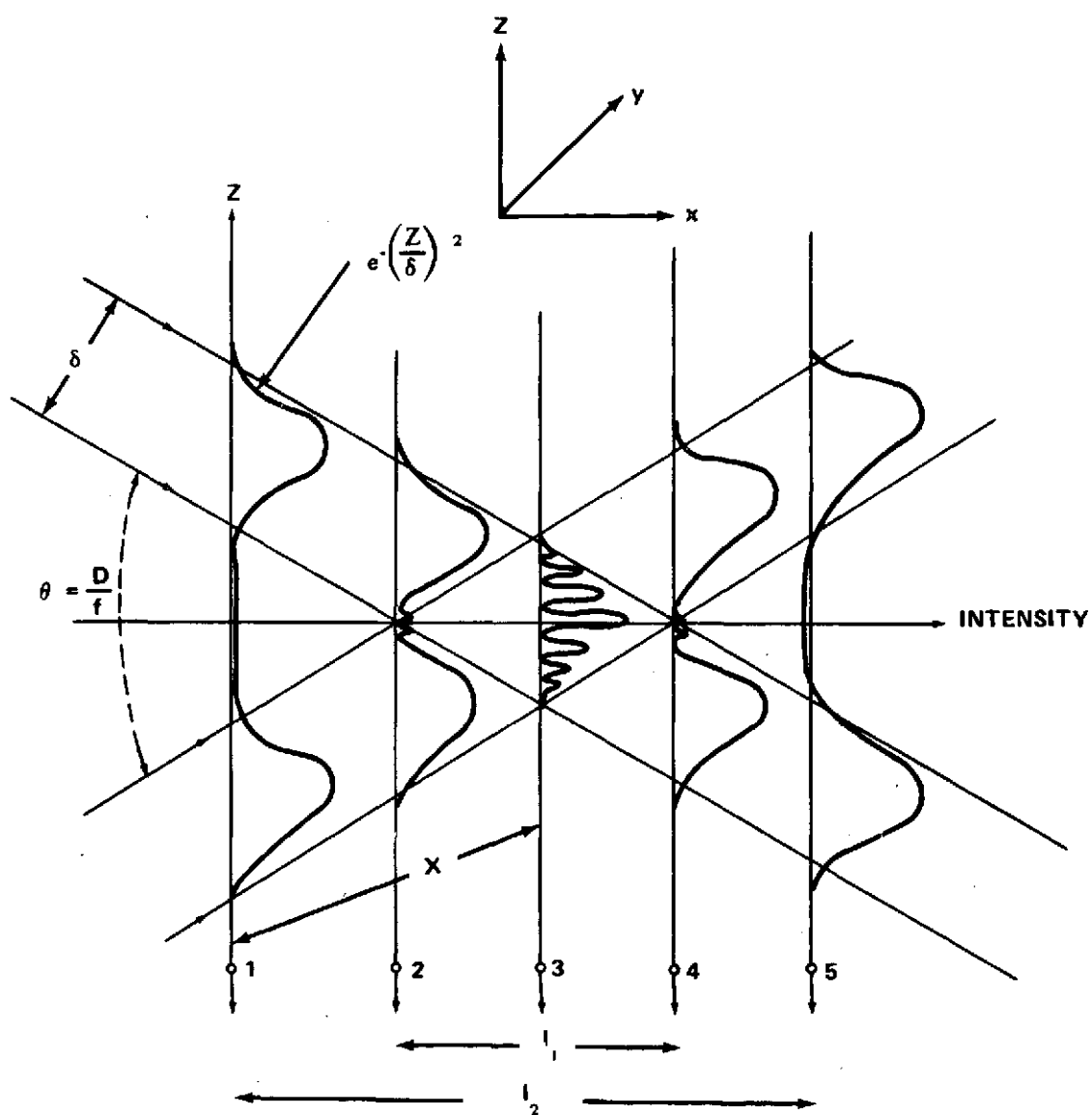


Figure 19. Schematic of intensity patterns for particles passing through various regions of the dual beam system.

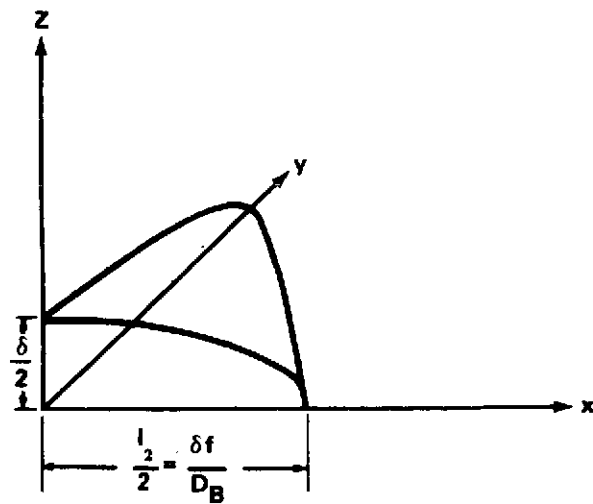


Figure 20. Shape of one-fourth of the crossover region in three dimensions for the cylindrical focusing lens.

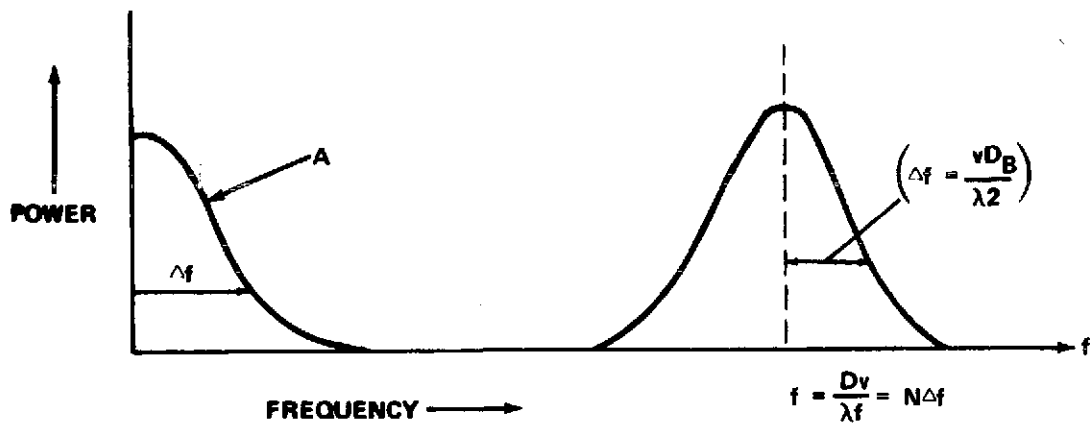


Figure 21. The power spectrum.

TABLE 1. VALUES OF S/N FOR VARIOUS SIZE PARTICLES

No.	$d_{\mu m}$ (microns)	$Q(x)$	v cm/sec	N_{ph}	η_{QM}	$N_e = N_{ph} \times \eta_{QM}$	$S/N = \sqrt{N_e}$
1.	3.0	~ 2	10^3	5×10^6	0.01	5×10^4	225
			1.0	5×10^9			
			0.1	5×10^{10}			
2.	1.0	~ 2	10^3	6×10^4	.01	6×10^2	24.5
			1.0	6×10^7			
			0.1	6×10^8			
3.	0.3	~ 1.0	10^3	2.5×10^2	.01	02.5	1.6
			1.0	2.5×10^5			
			0.1	2.5×10^6			

REFERENCES

1. Deepak, A., A Stokes' Velocity Photographic Method for Measuring the Size Distribution of Aerosols. NASA-TM X-64838; 1974.
2. Stokes, G. G.: Trans. Cambridge Phil. Soc., 9, No. 8, (1851).

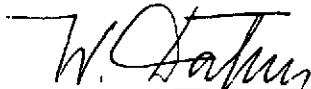
APPROVAL

A STANDARD PARTICLE SIZER - VELOCIMETER

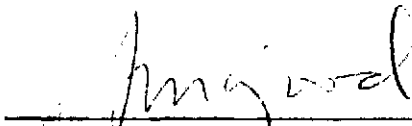
By Adarsh Deepak, R. Ozarski, and J. A. L. Thomson

The information in this report has been reviewed for security classification. Review of any information concerning Department of Defense or Atomic Energy Commission programs has been made by the MSFC Security Classification Officer. This report, in its entirety, has been determined to be unclassified.

This document has also been reviewed and approved for technical accuracy.



W. K. DAHM
Chief, Aerophysics Division



J. A. LOVINGOOD
Director, Systems Dynamics Laboratory